PP2A:B56 Regulates Meiotic Chromosome Segregation in *C. elegans* Oocytes

Laura Bel Borja[1], Flavie Soubigou[1], Samuel J.P. Taylor[1], Conchita Fraguas Bringas[1], Jacqueline Budrewicz[2,3], Pablo Lara-Gonzalez[2,3], Christopher G. Sorensen-Turpin[4], Joshua N. Bembenek[5], Dhanya K. Cheerambathur[6], and Federico Pelisch[1,✉]

[1]Centre for Gene Regulation and Expression, Sir James Black Centre, School of Life Sciences, University of Dundee. Dundee, DD1 5EH, United Kingdom
[2]Ludwig Institute for Cancer Research, San Diego, California, 92093, USA
[3]Department of Cellular and Molecular Medicine, University of California at San Diego, La Jolla, California, 92093, USA
[4]Department of Biochemistry, Cellular and Molecular Biology, University of Tennessee, 1414 Cumberland Avenue, Knoxville, TN 37996, USA
[5]Department of Molecular, Cellular, and Developmental Biology, University of Michigan. 1105 North University Ave., Ann Arbor, MI 48109-1085, USA
[6]Wellcome Centre for Cell Biology Institute of Cell Biology, School of Biological Sciences, The University of Edinburgh, Edinburgh, EH9 3BF, UK

During cell division, a balance between protein kinases and phosphatases is required to achieve specific and highly regulated phosphorylation levels. Protein Phosphatase 2A (PP2A) is a heterotrimeric enzyme composed of Scaffold (A), Catalytic (C), and Regulatory (B) subunits. PP2A can be targeted to different locations by specific interactions with one of several possible B subunits. B56-type subunits play important roles during meiosis in yeast and mice, including the protection of centromeric cohesion (targeted by Shugoshin) and kinetochore-microtubule attachments (targeted by BubR1). Protection of sister chromatid cohesion during meiosis I in *Caenorhabditis elegans* (*C. elegans*) does not involve the classic Shugoshin-dependent pathway and the *C. elegans* BubR1 orthologue Mad3^{SAN-1} lacks the PP2A-recruiting domain. We exploited these features to address the role(s) and regulation of PP2A:B56 during *C. elegans* oocyte meiosis. We report here that PP2A:B56 is recruited to chromosomes and spindle and is essential for proper chromosome segregation during oocyte meiosis in C. elegans. Recruitment of PP2A:B56 is regulated temporally and spatially by the kinase BUB-1 and is dependent on a previously unrecognised LxxIxE short linear motif (SLiM) in BUB-1. Our results highlight a novel, BUB-1-dependent mechanism for PP2A:B56 recruitment, essential for proper chromosome segregation during meiosis I.

meiosis | PP2A | Bub1 | oocytes | *C. elegans* | chromosome segregation
Correspondence: *f.pelisch@dundee.ac.uk*

Introduction

Formation of a diploid embryo requires that sperm and egg contribute exactly one copy of each chromosome. The cell division in charge of reducing ploidy of the genome is meiosis, which involves two chromosome segregation steps after a single round of DNA replication (Marston and Amon, 2004; Ohkura, 2015). Female meiosis is particularly error-prone (Hassold and Hunt, 2001) which can lead to chromosomally abnormal embryos. Therefore, understanding the molecular events that guarantee proper chromosome segregation during female meiosis is of paramount relevance. Cell division is under tight control of post-translational modifications (PTMs), of which phosphorylation is the most studied. The balance between kinase and phosphatase activities play a central role but we still lack a clear picture of how this is achieved during meiosis, specially when compared to mitosis (Novak et al., 2010; Gelens et al., 2018).

Protein Phosphatase 2A (PP2A) is a heterotrimeric serine/threonine phosphatase composed of a catalytic subunit C (PPP2C), a scaffolding subunit A (PPP2R1) and a regulatory subunit B (PPP2R2-5) (Xu et al., 2006; Cho and Xu, 2007; Xu et al., 2008). While the core enzyme (A and C subunits) is invariant, diversity in PP2A holoenzyme composition arises from the different regulatory B subunits. Four families of B subunits have been characterised: B55 (B), B56 (B), PR72 (B), and Striatin (B) (Shi, 2009; Seshacharyulu et al., 2013; Moura and Conde, 2019). PP2A:B56 regulates the spindle assembly checkpoint (SAC) (Espert et al., 2014; Qian et al., 2017; Hayward et al., 2019; Vallardi et al., 2019), chromosome congression (Xu et al., 2013; Xu et al., 2014), and centromeric cohesion (Kitajima et al., 2006; Riedel et al., 2006; Tang et al., 2006).

PP2A:B56 can be targeted to distinct sites by different proteins and two mechanisms have been characterised at the structural level. While an N-terminal coiled coil domain in Shugoshin/MEI-S332 binds PP2A:B56 (Xu et al., 2009), other substrates and/or regulatory proteins contain short linear motifs (SLiMs) following the consensus LxxIxE, which interact directly with B56 subunits (Van Roey and Davey, 2015; Hertz et al., 2016; Wang et al., 2016). BubR1 is one of the most widely studied LxxIxE-containing proteins, and has been thoroughly characterised during mitosis, where it plays a role in targeting PP2A:B56 to kinetochores (Foley et al., 2011; Suijkerbuijk et al., 2012; Kruse et al., 2013). BubR1 is also required during meiosis (Homer et al., 2009; Touati et al., 2015; Yoshida et al., 2015) where kinetochore-microtubule attachments are stabilized by counteracting Aurora B/C activity through kinetochore dephosphorylation by PP2A:B56 (Yoshida et al., 2015). It is important to notice that mutations in the B56-targeting sequence in BubR1 do not completely inhibit PP2A:B56ϵ localisation (Yoshida et al., 2015), which could suggest the existence of additional recruitment mechanisms.

While PP2A is important for proper centrosome function during mitosis in *C. elegans* (Schlaitz et al., 2007; Kitagawa et al., 2011; Song et al., 2011), its function during meiosis remains obscure. During oocyte meiosis I, another major phosphatase, Protein Phosphatase 1 (PP1), initiates disas-

sembly of kinetochore complexes to promote elongation of the acentrosomal spindle during anaphase (Hattersley et al., 2016). However, the nematode Aurora B orthologue, AIR-2, localises exclusively between homologous chromosomes (Schumacher et al., 1998; Kaitna et al., 2002; Rogers et al., 2002), away from kinetochores, indicating that PP1 is unlikely to be the main phosphatase counteracting Aurora B. The core components of the PP2A holoenzyme in *C. elegans* are LET-92 (catalytic C subunit) and PAA-1 (scaffolding A subunit), and the regulatory B subunits are B55^{SUR-6} (Sieburth et al., 1999), B56^{PPTR-1} and B56^{PPTR-2} (Padmanabhan et al., 2009), B72^{RSA-1} (Schlaitz et al., 2007), and CASH-1/Striatin (Pal et al., 2017). Interestingly, the closest *C. elegans* BubR1 orthologue Mad3^{SAN-1}, does not localise to unattached kinetochores (Essex et al., 2009) and lacks the domain responsible for PP2A:B56 targeting. Additionally, the *C. elegans* Shugoshin orthologue, SGO-1, is dispensable for protection of cohesin in meiosis I (de Carvalho et al., 2008), for the Aurora B-targeting histone H3T3 phosphorylation (Ferrandiz et al., 2018), and depletion or a mutant allele of SGO-1 do not show any clear mitotic defect (Kim et al., 2015). These observations further suggest the existence of additional unknown mechanisms of PP2A regulation.

In the present work, we used *C. elegans* oocytes to establish the role and regulation of PP2A during female meiosis. We found that PP2A is essential for female meiosis and its recruitment to meiotic chromosomes and spindle is mediated by the B56 regulatory subunits PPTR-1 and PPTR-2. Targeting of the B56 subunits is mediated by the kinase BUB-1 through a canonical B56 LxxIxE motif which targets both PPTR-1 and PPTR-2 to the chromosomes and central-spindle during meiosis. Overall, we provide evidence for a novel, BUB-1-regulated role for PP2A:B56 during female meiosis. We propose that PP2A is the main phosphatase counteracting Aurora B-mediated phosphorylation to achieve proper phosphorylation levels during meiosis I.

Results

Protein Phosphatase 2A is essential for spindle assembly and chromosome segregation during meiosis I. We used dissected *C. elegans* oocytes to assess the role and regulation of PP2A activity during female meiosis by following spindle and chromosome dynamics using GFP-tagged tubulin and mCherry-tagged histone (see Figure 1A for PP2A schematic) During meiosis I, six pairs of homologous chromosomes (bivalents) are captured and aligned by an acentrosomal spindle, in order to segregate them. Chromosome segregation is associated with dramatic changes in microtubule organisation as anaphase progresses, with microtubule density decreasing in poles and the bulk of GFP::tubulin is detected in the central-spindle (Figure 1B; Supp. Movie 1). In sharp contrast, depletion of the PP2A catalytic subunit LET-92 drastically affects meiosis I. While bivalent structure appears normal, chromosomes fail to align in 80% of the oocytes, compared to 6% in wild type (Figure 1B, cyan arrow; P<0.0001, Fisher's exact test, Figure 1C). During anaphase, chromosomes collapse into a small area where, in some cases, a separation of two masses was apparent for a short time (Figure 1B, yellow arrow). Lastly, and regardless of whether these two masses were observed, only 23% of let-92(RNAi) oocytes achieved polar body extrusion, compared to 100% in wild type (P<0.0001, Fisher's exact test, Figure 1D). Similar defects were observed by depleting the sole PP2A scaffold subunit, PAA-1 (Figure S1A). Regarding the spindle, microtubules do not organise into a bipolar structure in the absence of PP2A (Figure 1B, magenta arrows and Figure S1A).

We then sought to determine whether the lack of chromosome segregation was due to a defect in meiosis I progression. We measured endogenously GFP-tagged Securin^{IFY-1} levels as a readout for Anaphase Promoting Complex/Cyclosome (APC/C) activity (i.e. anaphase progression). Cytoplasmic Securin^{IFY-1} degradation proceeded at similar rates in wild type and LET-92-depleted oocytes (Figure 1E and F; Supp. Movie 2), indicating that APC/C activity is largely unperturbed in the absence of PP2A. Taken together, we have found that PP2A is required for chromosome segregation during meiosis I.

PP2A:B56 localises to meiotic chromosomes and spindle. To assess the localisation of the core PP2A enzyme (A and C subunits) in vivo we attempted to tag endogenous LET-92 with GFP but were unsuccessful, presumably due to disruption of its native structure, in agreement with a recent report (Magescas et al., 2019) and with previous efforts to express recombinant tagged PP2A catalytic subunit (Cho and Xu, 2007). We thus generated a GFP-tagged version of the sole *C. elegans* PP2A scaffold subunit, PAA-1, and used this to assess the localisation of the core enzyme (Figure 2A; Supp. Movie 3). In agreement with previous immunofluorescence data, the fusion protein localised in centrosomes and P-granules during the early embryonic mitotic divisions (Lange et al., 2013, Figure S1C). During meiosis I, GFP::PAA-1 localises to the acentrosomal spindle poles (Figure 2A, cyan arrows), between homologous chromosomes (Figure 2A, magenta arrows), and faintly to the characteristic holo-kinetochores/chromosomes (Figure 2A, yellow arrows). As meiosis I progresses, GFP::PAA-1 signal concentrates in the central-spindle between the segregating chromosomes (Figure 2A, magenta arrowhead), finally disappearing by late anaphase I. This pattern differs substantially from that of Protein Phosphatase 1 (PP1) which localises in the characteristic cup-shaped holo-kinetochores (Hattersley et al., 2016). This indicates that PP1 and PP2A are recruited to specific sites which, together with substrate specificity, could be key in specifying their respective roles during meiosis.

To address which regulatory subunits are involved in targeting PP2A to the meiotic spindle and chromosomes, we first assessed the localisation of the two *C. elegans* B56 orthologues, PPTR-1 and PPTR-2 and the single B55 ortho-

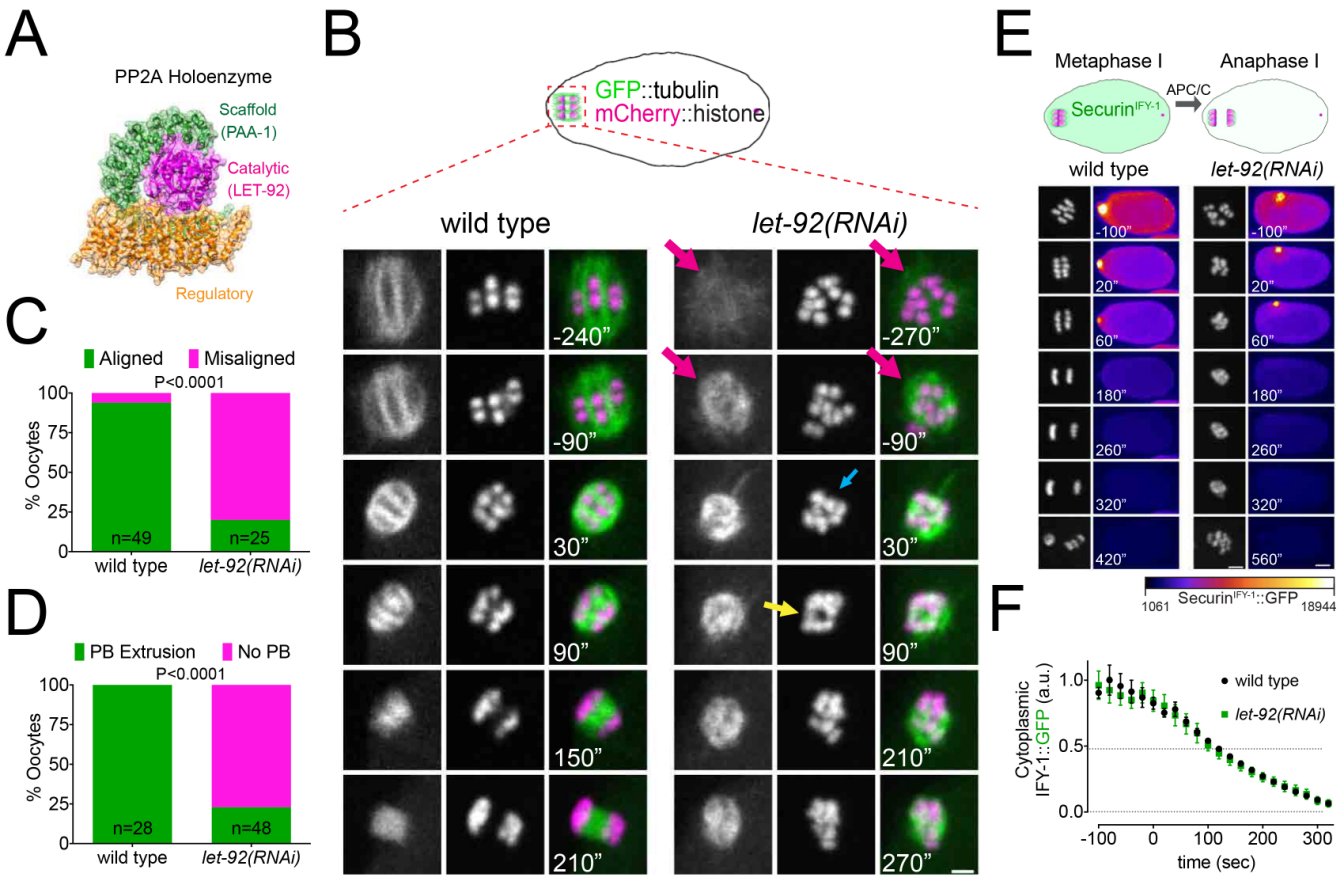

Fig. 1. PP2A is essential for Meiosis I in C. elegans oocytes. A. Schematic of the PP2A heterotrimer highlighting the single catalytic and scaffold subunits in *C. elegans* (LET-92 and PAA-1, respectively). The schematic was generated from the PDB structure 2npp (Xu et al., 2006). **B.** Microtubule and chromosome dynamics were followed in wild type and *let-92(RNAi)* oocytes expressing GFP::tubulin and mCherry::histone. Magenta arrows point to defective spindle structure; the cyan arrow points to misaligned chromosomes; the yellow arrow shows an apparent separation between chromosome masses. Inset numbers represent the time relative to metaphase I in seconds. See also Supp. Movie 1. Scale bar, 2µm. **C.** The number of oocytes with missaligned chromosomes at metaphase I in wild type and *let-92(RNAi)* oocytes was analysed and the percentage is represented (P<0.0001, Fisher's exact test). **D.** The number of oocytes with an extruded polar body after meiosis I in wild type and *let-92(RNAi)* oocytes was analysed and the percentage is represented (P<0.0001, Fisher's exact test). **E.** Securin^{IFY-1} degradation was used as a proxy for anaphase progression and followed in wild type and *let-92(RNAi)* oocytes. Greyscale images of the chromosomes are shown as well as whole oocyte images using the 'fire' LUT. The intensity scale is shown in the bottom. Inset numbers represent the time relative to metaphase I in seconds. See also Supp. Movie 2. Scale bar, 2µm. **F.** Cytoplasmic Securin^{IFY-1} levels were measured throughout meiosis I and the mean ± s.e.m is shown in the graph.

logue, SUR-6 (Figure S2A). Live imaging of endogenous, GFP-tagged regulatory subunits revealed that both B56 orthologues, PPTR-1 and PPTR-2, localised strongly and dynamically within the meiotic spindle whereas no spindle or chromosome localisation of B55^{SUR-6} could be detected (Figure S2B). PPTR-1 has the highest sequence identity with human B56α2 (68.3%) and ϵ3 (71.87%) whereas PPTR-2 displays the highest sequence identity with human B56δ3 and B56γ1 (68.97%) (Table 1 and Supp. Table 1).

	PPTR-1	B56β1	B56ε3	B56α2	PPTR-2	B56δ3	B56γ1
PPTR-1		60.12	71.87	68.30	52.26	60.17	64.48
PPTR-2	52.26	56.36	63.94	60.84		66.19	68.97

Table 1. Sequence identity between full-length mammalian B56 isoforms and *C.elegans* orthologues PPTR-1 and PPTR-2. Table was created using Clustal Omega version 2.1. See Supplementary Table 1 for full Percent Identity Matrix.

Focusing on a C-terminal sequence in B56 which plays a key role in specifying centromere versus kinetochore localisation (Vallardi et al., 2019), further confirmed that PPTR-1 displays the highest sequence identity with the centromeric B56s, α and ϵ (93.75% and 87.5% respectively), while PPTR-2 displays the highest sequence identity with the kinetochore-localised B56, γ and δ (93.75% and 100%) (Figure S2C). We will henceforth refer to PPTR-1 as B56α^{PPTR-1} and to PPTR-2 as B56γ^{PPTR-2}. We used endogenous GFP-tagged versions of B56α^{PPTR-1} and B56γ^{PPTR-2} (Kim et al., 2017) and analysed their dynamic localisation pattern in greater spatial and temporal detail. B56α^{PPTR-1} localises mainly to the region between homologous chromosomes (midbivalent) during metaphase of meiosis I (Figure 2B, orange arrows; Supp. Movie 4) and faintly in kinetochores (Figure 2B, cyan arrows). During anaphase I, B56α^{PPTR-1} is present exclusively on the central spindle (Figure 2B; Supp. Movie 4). Like its paralog, B56γ^{PPTR-2} localises mainly in the midbivalent during metaphase of meiosis I (Figure 2C, orange arrows; Supp. Movie 5) and faintly in kinetochores and/or chromosomes (Figure 2C, cyan arrows). A difference between the two paralogs arises during anaphase: B56γ^{PPTR-2} is present in the central spindle and also on chromosomes (Figure 2C; Supp. Movie 5). In spite of this difference, the levels of B56α^{PPTR-1} and B56γ^{PPTR-2} within the

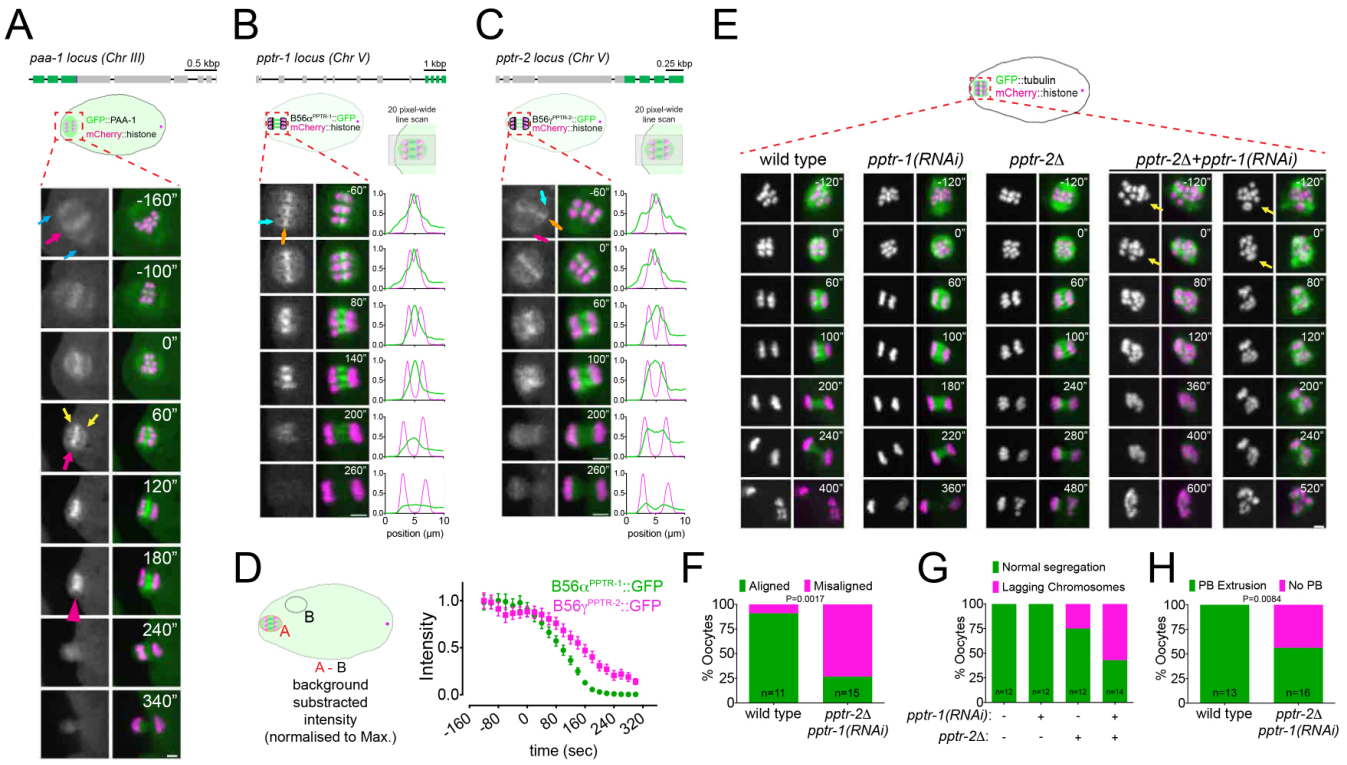

Fig. 2. ***C. elegans*** **B56 regulatory subunits PPTR-1 and PPTR-2 are required for normal Meiosis I. A.** Top, Schematic of the *paa-1* gene structure and its tagging with *gfp*. Bottom, the PP2A scaffold subunit GFP::PAA-1 was followed throughout meiosis I in a dissected oocyte. Magenta arrows point to the midbivalent; the cyan arrows point to spindle poles; yellow arrows highlight the chromosome-associated/kinetochore localisation. Inset numbers represent the time relative to metaphaseI in seconds. See also Supp. Movie 3. Scale bar, 2 µm. **B.** Top, Schematic of the *pptr-1* gene structure and its tagging with *gfp*. Bottom, PPTR-1 and chromosome dynamics were followed in oocytes expressing PPTR-1::GFP and mCherry::histone. The orange arrow points to the midbivalent and the cyan arrow points to the kinetochore. Inset numbers represent the time relative to metaphaseI in seconds. See also Supp. Movie 4. Scale bar, 2 µm. Representative, spindle-wide (20 pixels) line profiles are shown on the right of each time point. **C.** Top, Schematic of the *pptr-2* gene structure and its tagging with gfp. Bottom, PPTR-2 and chromosome dynamics were followed in oocytes expressing PPTR-1::GFP and mCherry::histone. The orange arrow points to the midbivalent and the cyan arrow points to the kinetochore. Inset numbers represent the time relative to metaphaseI in seconds. See also Supp. Movie 5. Scale bar, 2 µm. Representative, spindle-wide (20 pixels) line profiles are shown on the right of each time point. **D.** PPTR-1::GFP and PPTR-2::GFP levels were measured throughout meiosis I and the mean ± s.e.m is shown in the graph. **E.** Microtubule and chromosome dynamics were followed in wild type, *pptr-2Δ*, *pptr-1(RNAi)*, and *pptr-2Δ/pptr-1(RNAi)* oocytes expressing GFP::tubulin and mCherry::histone. Inset numbers represent the time relative to metaphase I in seconds. See also Supp. Movie 6. Scale bar, 2 µm. **F.** The number of oocytes with misaligned chromosomes at metaphase I in wild type and *pptr-2Δ/pptr-1(RNAi)* oocytes was analysed and the percentage is represented (P=0.0017, Fisher's exact test). **G.** The number of oocytes with lagging chromosomes during Anaphase I in wild type, *pptr-1(RNAi)*, *pptr-2Δ* , and *pptr-2Δ/pptr-1(RNAi)* oocytes was analysed and the percentage is represented. Comparisson between wild type and pptr-2Δ/pptr-1(RNAi) oocytes was done using the Fisher's exact test (P=0.0022). **H.** The number of oocytes with an extruded polar body after meiosis I in wild type and *pptr-2Δ/pptr-1(RNAi)* oocytes was analysed and the percentage is represented (P=0.0084, Fisher's exact test).

meiotic spindle follow similar dynamics (Figure 2D).

These results show that *C. elegans* B56 subunits, like their mammalian counterparts, display a similar but not identical localisation pattern: while both B56$\alpha^{\text{PPTR-1}}$ and B56$\gamma^{\text{PPTR-2}}$ are present in the midbivalent and central spindle, B56$\gamma^{\text{PPTR-2}}$ is also associated with chromosomes during anaphase.

Depletion of B56$\alpha^{\text{PPTR-1}}$ and B56$\gamma^{\text{PPTR-2}}$ leads to severe meiotic defects. To address the role of the *C. elegans* B56 subunits during meiosis I, we used a B56$\gamma^{\text{PPTR-2}}$ deletion allele (*ok1467, 'pptr-2Δ'*) and RNAi-mediated depletion of B56$\alpha^{\text{PPTR-1}}$ ('pptr-1(RNAi)'). Double B56$\alpha^{\text{PPTR-1}}$/B56$\gamma^{\text{PPTR-2}}$ depletion had a severe impact on meiosis I (Figure 2E-H; Supp. Movie 6). In spite of having normal total tubulin levels (Figure S3), oocytes failed to assemble a proper bipolar spindle (Figure 2E, yellow arrows). Chromosome alignment was also affected: 73% of B56$\alpha^{\text{PPTR-1}}$/B56$\gamma^{\text{PPTR-2}}$-depleted oocytes had misaligned chromosomes at metaphase of meiosis I, compared to 9% in wild type (P=0.0017, Fisher's exact test, Figure 2F). Additionally, 57% of B56$\alpha^{\text{PPTR-1}}$/B56$\gamma^{\text{PPTR-2}}$-depleted oocytes had lagging chromosomes (Figure 2G) while 44% failed to extrude the polar body during meiosis I, compared to 0% in wild type (P=0.0084, Fisher's exact test, Figure 2H). Taken together, these results indicate that PP2A:B56 is essential for accurate chromosome segregation during meiosis I. Additionally, B56$\alpha^{\text{PPTR-1}}$ and B56$\gamma^{\text{PPTR-2}}$ are acting, at least partially, in a redundant way.

BUB-1 targets B56 subunits through a L-x-x-I-x-E motif. We next sought to identify the protein(s) involved in targeting PP2A:B56 to the meiotic spindle and chromosomes. We initially focused our attention on the *C. elegans* Shugoshin orthologue, SGO-1, and the BubR1 orthologue, Mad3$^{\text{SAN-1}}$. GFP::Mad3$^{\text{SAN-1}}$ is not detected in meiotic chromosomes or spindle (Figure S4A) and Mad3$^{\text{SAN-1}}$ depletion by RNAi (*'san-1(RNAi)'*) or using a Mad3$^{\text{SAN-1}}$ deletion allele (*ok1580, 'san-1Δ'*) does not affect B56$\alpha^{\text{PPTR-1}}$

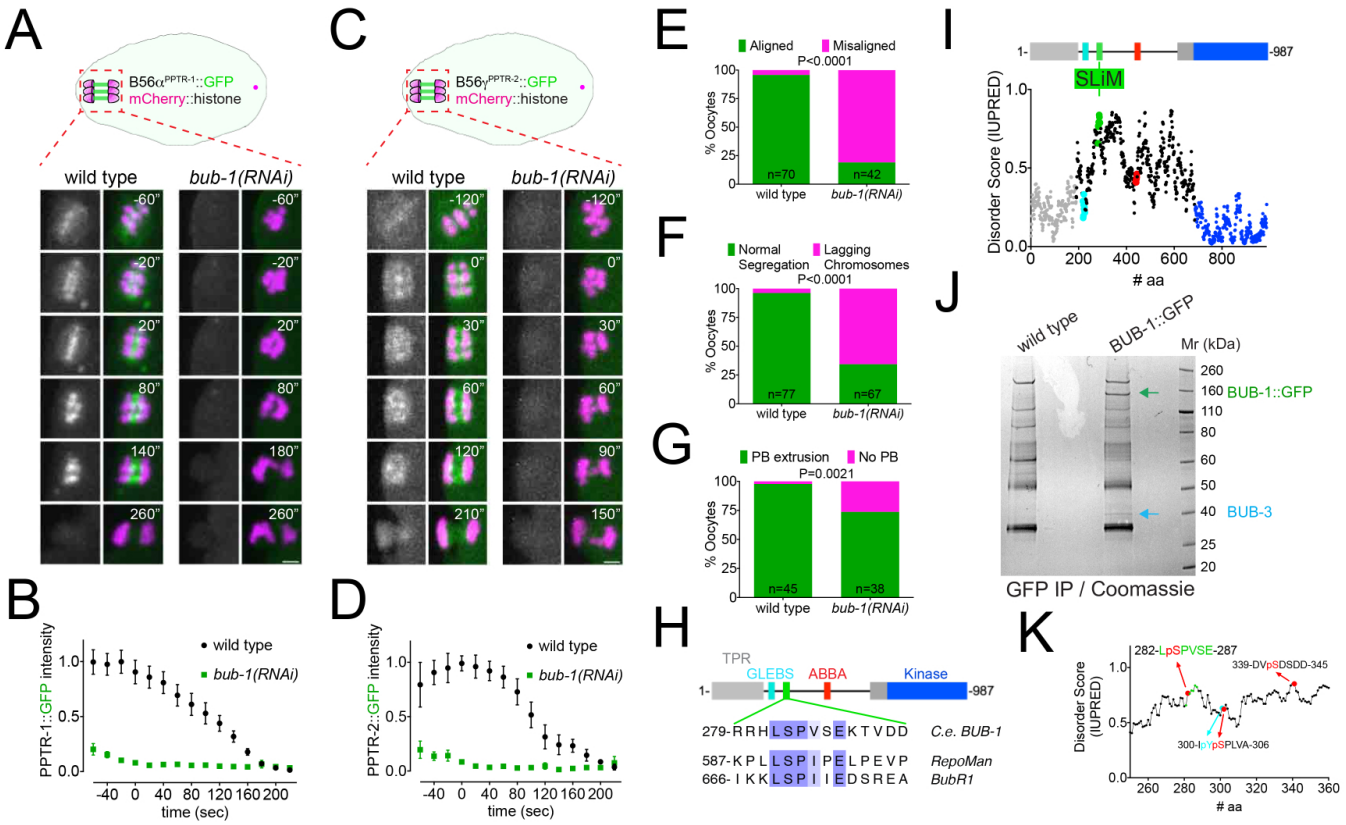

Fig. 3. BUB-1 recruits B56α^{PPTR-1} and B56γ^{PPTR-2} during oocyte meiosis. A. B56α^{PPTR-1} and chromosome dynamics were followed in wild type and *bub-1(RNAi)* oocytes expressing PPTR-1::GFP and mCherry::histone. See also Supp. Movie 9. Scale bar, 2 µm. **B.** PPTR-1::GFP levels were measured in wild type and *bub-1(RNAi)* oocytes throughout meiosis I and the mean ± s.e.m is shown in the graph. **C.** B56γ^{PPTR-2} and chromosome dynamics were followed in wild type and *bub-1(RNAi)* oocytes expressing PPTR-2::GFP and mCherry::histone. See also Supp. Movie 10. Scale bar, 2 µm. **D.** PPTR-2::GFP levels were measured in wild type and *bub-1(RNAi)* oocytes throughout meiosis I and the mean ± s.e.m is shown in the graph. **E.** The number of oocytes with missaligned chromosomes at metaphaseI in wild type and *bub-1(RNAi)* oocytes was analysed and the percentage is represented (P<0.0001, Fisher's exact test). **F.** The number of oocytes with lagging chromosomes during anaphase I in wild type and *bub-1(RNAi)* oocytes was analysed and the percentage is represented (P<0.0001, Fisher's exact test). **G.** The number of oocytes with an extruded polar body after meiosis I in wild type and *bub-1(RNAi)* oocytes was analysed and the percentage is represented (P=0.0021, Fisher's exact test). **H.** C. elegans BUB-1 LxxIxE SLiM is shown aligned with BubR1 and Repoman SLiMs. The only change within the LxxIxE sequence itself is the presence of a valine instead of isoleucine, which still fits within the consensus (Wang et al., 2016). The alignment was performed using Clustal Omega and visualised with Jalview (Waterhouse et al., 2009). **I.** Disorder prediction of full-length BUB-1 was done using IUPRED2A (Erdős and Dosztányi, 2020). All prevuously characterised BUB-1 domains fall within ordered regions (<0.5). The putative SLiM is in a disordered region (IUPRED score ≈0.8). **J.** BUB-1::GFP was immunoprecipitated and the eluted proteins were run on SDS-PAGE followed by coomassie staining. The position of BUB-1::GFP and BUB-3 are highlighted with green and blue arrows, respectively. The band corresponding to BUB-1::GFP was further analysed by mass spectrometry to look for phospho-modified peptides. **K.** Serine 283 is phosphorylated in vivo. In addition, three other phosphorylation sites were identified within this disordered region.

(Figure S4B) or B56γ^{PPTR-2} (Figure S4C, Supp. Movie 7). We then turned our attention to the single *C. elegans* Shugoshin^{SGO-1}. RNAi-mediated depletion of SGO-1 did not reduce B56α^{PPTR-1} levels (Figure S4D) or B56γ^{PPTR-2} (Figure S4E, Supp. Movie 8). Hence, Mad3^{SAN-1} and Shugoshin^{SGO-1} are not involved in PP2A:B56 targeting during meiosis in *C. elegans* oocytes.

C. elegans B56 subunits display a dynamic localisation pattern similar to that of the kinase BUB-1 throughout meiosis I (Monen et al., 2005; Dumont et al., 2010; Pelisch et al., 2017; Pelisch et al., 2019). Since Bub1 and BubR1 are paralogous proteins involved in the spindle assembly checkpoint (Bolanos-Garcia and Blundell, 2011; Elowe, 2011; Nilsson, 2015), we tested whether BUB-1 recruits B56 subunits in the absence of a functional BubR1. RNAi-mediated depletion of BUB-1 abolished localisation of B56α^{PPTR-1} (Figure 3A and B; Supp. Movie 9) and B56γ^{PPTR-2} (Figure 3C and D; Supp. Movie 10). In contrast, BUB-1 depletion does not affect the localisation of the catalytic subunit of another major phosphatase, PP1^{GSP-2} (Figure S5; Supp. Movie 11). Interestingly, BUB-1 depletion shares some phenotypes with PP2A depletion such as chromosome alignment defects (Figure 3E), lagging chromosomes (Figure 3F), and a small but significant defect in polar body extrusion (Figure 3G), in agreement with previous data (Dumont et al., 2010; Laband et al., 2017; Pelisch et al., 2019). *C. elegans* BUB-1 contains a conserved N-terminal tetratricopeptide repeat (TPR) domain, a C-terminal kinase domain, and regions mediating its interaction with Cdc20 and BUB3 (ABBA and GLEBS motifs, respectively) (Figure 3H; Moyle et al., 2014; Kim et al., 2015; Kim et al., 2017). Sequence analysis of *C. elegans* BUB-1 revealed the presence of a putative B56 LxxIxE motif in residues 282-287 (Figure 3H). When compared with two well-characterised LxxIxE motif-containing proteins, BubR1 and RepoMan, there is a high degree of conservation in the key residues making contacts with the B56 hydrophobic pockets (Figure 3H). In addition, the SLiM-

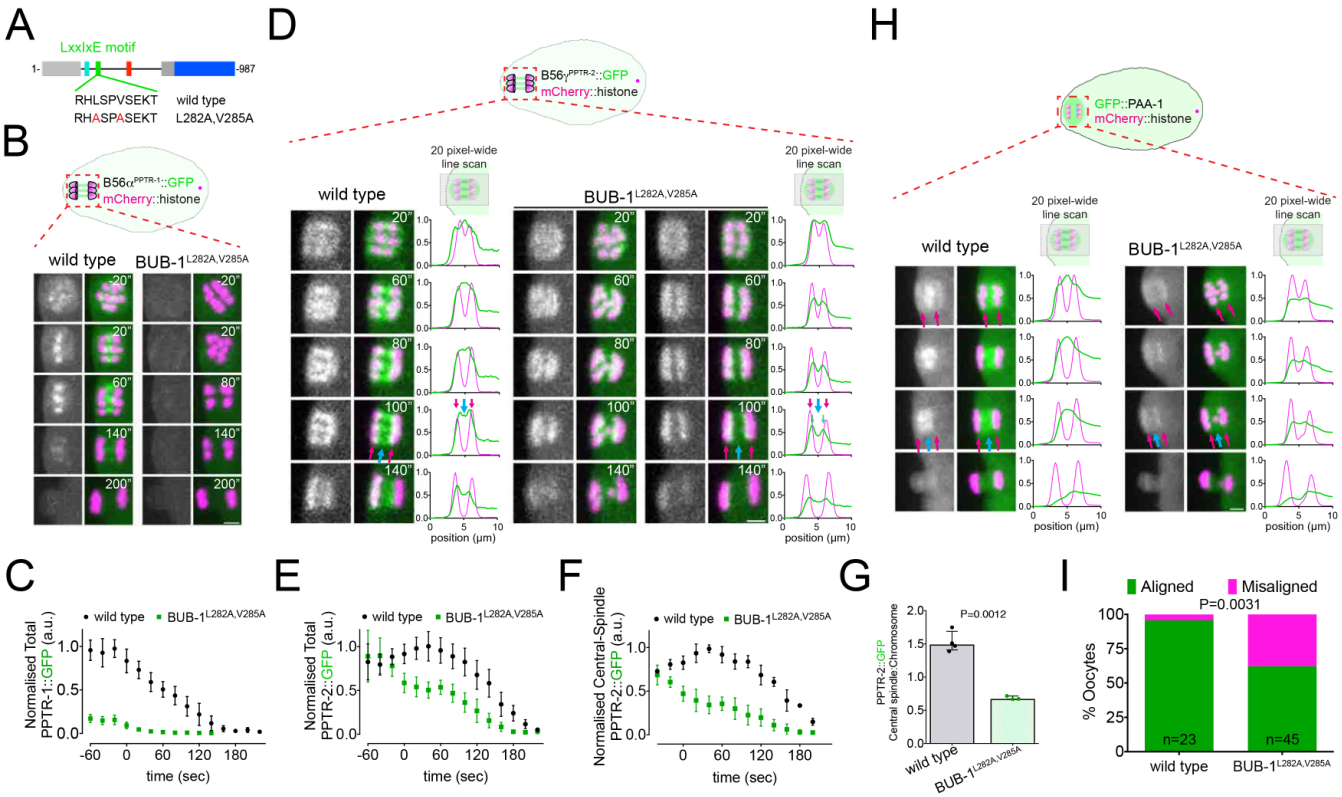

Fig. 4. B56α^{PPTR-1} and B56γ^{PPTR-2} are targeted through a LxxIxE motif in BUB-1. A. Schematic showing the LxxIxE motif in BUB-1 and the BUB-1^{L282A,V285A} mutant. **B.** B56α^{PPTR-1} and chromosome dynamics were followed in wild type and in BUB-1^{L282A,V285A} oocytes expressing PPTR-1::GFP and mCherry::histone. See also Supp. Movie 12. Scale bar, 2 µm. **C.** PPTR-1::GFP levels were measured in wild type and BUB-1^{L282A,V285A} oocytes throughout meiosis I and the mean ± s.e.m is shown in the graph. **D.** B56γ^{PPTR-2} and chromosome dynamics were followed in wild type and in BUB-1^{L282A,V285A} oocytes expressing PPTR-2::GFP and mCherry::histone. Magenta arrows point towards chromosomes whereas cyan arrows point towards the central spindle. See also Supp. Movie 13. Scale bar, 2 µm. Representative, spindle-wide line profiles are shown on the right of the images for each time point. **E.** PPTR-2::GFP levels were measured in wild type and BUB-1^{L282A,V285A} oocytes throughout meiosis I and the mean ± s.e.m is shown in the graph. **F.** Midbivalent/Central spindle PPTR-2::GFP levels were measured in wild type and BUB-1^{L282A,V285A} oocytes throughout meiosis I and the mean ± s.e.m is shown in the graph. **G.** The graph shows the ratio between central spindle and chromosomal PPTR-2::GFP intensities measured at 40 seconds after metaphase I. The graph represents the median and the interquartile range and individual points are also shown (P=0.0012, two-tailed unpaired t-test with Welch's correction). **H.** GFP::PAA-1 is present on chromosomes in the BUB-1^{L282A,V285A} mutant. PAA-1 and chromosome dynamics were followed in wild type and in BUB-1^{L282A,V285A} oocytes expressing GFP::PAA-1 and mCherry::histone. Representative, spindle-wide line profiles are shown on the right of the images for each time point. Scale bar, 2 µm. **I.** The number of oocytes with missaligned chromosomes at metaphaseI in wild type and BUB-1^{L282A,V285A} oocytes was analysed and the percentage is represented (P=0.0031, Fisher's exact test).

binding B56 hydrophobic pocket is very well conserved in *C. elegans* (Figure S6). The LxxIxE SLiM lies within a region of BUB-1 predicted to be disordered (Figure 3I) and serine 283 embedded in the putative SLiM lies within a Cdk1 Ser/Thr-Pro motif. When this serine is phosphorylated in other well characterised LxxIxE motifs, it increases the affinity for B56 by ≈10-fold (Wang et al., 2016). To determine if Ser 283 was phosphorylated in vivo, we immunoprecipitated endogenous, GFP-tagged BUB-1 from embryo lysates using a GFP nanobody. Immunoprecipitated material was digested with trypsin, peptides analysed by mass spectrometry and searches conducted for peptides containing phosphorylated adducts. As expected GFP-tagged, but not untagged, BUB-1 was pulled down by the GFP nanobody (Figure S7A) along with the BUB-1 partner, BUB-3 (Figure 3J, blue arrow). After a search for phosphorylated residues, we found four sites clustered within a disordered region, one of which is Ser 283, within the putative B56 SLiM (Figure 3K; see also representative MS spectra in Figure S7B).

To determine the importance of the putative LxxIxE motif in PP2A:B56 recruitment by BUB-1, we mutated two key hydrophobic residues (Wang et al., 2016) in endogenous BUB-1, Leu 282 and Val 285 to Ala ('BUB-1^{L282A,V285A}', Figure 4A). While localisation of BUB-1^{L282A,V285A} was indistinguishable from that of wild type BUB-1 (Figure S8A), localisation of B56α^{PPTR-1} to the midbivalent and central spindle was almost completely lost in the BUB-1^{L282A,V285A} mutant (Figure 4B, C; Supp. Movie 12). We then analysed B56γ^{PPTR-2} and found that its midbivalent and central-spindle localisation were also dependent on the BUB-1 LxxIxE motif (Figure 4D, cyan arrows, and 4E, F; Supp. Movie 13). In contrast, chromosome-associated B56γ^{PPTR-2} was less affected in the BUB-1^{L282A,V285A} mutant (Figure 4D, magenta arrows). To get a better measure of this phenomenon, we calculated the central-spindle/chromosome B56γ^{PPTR-2}::GFP ratio and found that it was decreased by 2.2-fold in BUB-1^{L282A,V285A} mutant oocytes (Figure 4G). BUB-1 LxxIxE motif mutation abrogates PP2A A subunit PAA-1 localisation in the midbivalent and central spindle (Figure 4H, cyan arrows). Some GFP::PAA-1 signal was still detected in anaphase chromosomes, likely through the remaining B56γ^{PPTR-2} on chromosomes (Figure 4H,

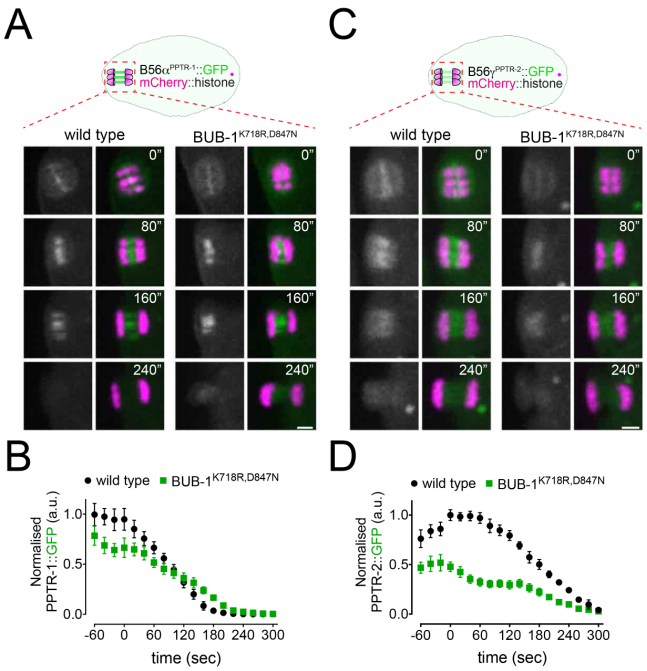

Fig. 5. Kinase domain-dependent, SLiM-independent recruitment of B56γ^{PPTR-2} to chromosomes by BUB-1. A. B56α^{PPTR-1} and chromosome dynamics were followed in wild type and BUB-1^{K718R,D847N} oocytes expressing PPTR-2::GFP and mCherry::histone. See also Supp. Movie 14. Scale bar, 2 µm. **B.** PPTR-1::GFP levels were measured in wild type and BUB-1^{K718R,D847N} oocytes throughout meiosis I and the mean ± s.e.m is shown in the graph. **C.** B56γ^{PPTR-2} and chromosome dynamics were followed in wild type and BUB-1^{K718R,D847N} oocytes expressing PPTR-2::GFP and mCherry::histone. See also Supp. Movie 15. Scale bar, 2 µm. **D.** PPTR-2::GFP levels were measured in wild type and BUB-1^{K718R,D847N} oocytes throughout meiosis I and the mean ± s.e.m is shown in the graph.

magenta arrows). This LxxIxE motif-dependent regulation is specific for B56 subunits because the localisation of the spindle assembly checkpoint component Mad1^{MDF-1}, which is a known BUB-1 interactor (Moyle et al., 2014), is not disrupted after mutating the BUB-1 LxxIxE motif (Figure S8B). We then focused our attention to chromosome dynamics and found that 38% of BUB-1^{L282A,V285A} mutant oocytes display chromosome alignment defects, compared to 4% in wild type (P=0.0031, Fisher's exact test, Figure 4I).

These results indicate that the BUB-1 LxxIxE motif recruits PP2A:B56 and plays an important role in chromosome alignment. Interestingly, the newly identified LxxIxE motif is specifically involved in midbivalent and central spindle B56 recruitment. These results also suggest that BUB-1 recruits B56 subunits mostly via an LxxIxE motif-dependent mechanism with some additional, SLiM-independent contribution.

BUB-1 recruits the chromosomal pool of B56γ^{PPTR-2} through its C-terminal kinase domain. Since not all of B56γ^{PPTR-2} is targeted by the BUB-1 LxxIxE motif, we turned our attention to BUB-1 kinase domain. In *C. elegans* BUB-1 kinase domain regulates its interaction with binding partners such as Mad1^{MDF-1}. The K718R/D847N double mutation (equivalent to positions K821 and D917 in human Bub1) destabilizes the kinase domain and prevents its interaction with Mad1^{MDF-1} (Moyle et al., 2014). We generated endogenous BUB-1^{K718R,D847N} and confirmed that these mutations abolish recruitment of Mad1^{MDF-1} (Figure S8B). B56α^{PPTR-1}::GFP localisation and dynamics remained largely unaltered in the mutant BUB-1^{K718R,D847N} (Figure 5A, B; Supp. Movie 14). In contrast, B56γ^{PPTR-2}::GFP levels were significantly reduced in the BUB-1^{K718R,D847N} mutant (Figure 5C, D; Supp. Movie 15). These results show that the BUB-1 kinase domain is important for recruitment of B56γ^{PPTR-2} but not of B56α^{PPTR-1}. Thus, BUB-1 is a key factor for the recruitment of PP2A:B56 but could also provide the basis for establishing (probably together with other proteins) the two pools of B56γ^{PPTR-2}.

Discussion

In the present manuscript, we uncovered a new role for PP2A during oocyte meiosis in *C. elegans*. PP2A regulates multiple aspects of meiosis I including spindle assembly, chromosome segregation, and polar body extrusion. Proper chromosome dynamics and polar body extrusion are mediated by B56 subunits. We have uncovered a new B56 LxxIxE motif in *C. elegans* BUB-1 that recruits PP2A:B56 and is important for chromosome alignment during meiosis I. This mechanism does not rely on Shugoshin or BubR1 and is independent of the spindle assembly checkpoint. These findings could have wider implications for PP2A:B56 targeting in other systems. For example, a putative LxxIxE has been identified in human Bub1 (Wang et al., 2016) and its possible that it could function redundantly with BubR1 to ensure PP2A recruitment during meiotic chromosome segregation.

Interestingly, while BUB-1 is present in the midbivalent and kinetochores, the LxxIxE motif-dependent pathway for B56 targeting is specific for the midbivalent. This also leads to a degree of B56 isoform-specific regulation by BUB-1: only the midbivalent/central-spindle subpopulation of B56γ^{PPTR-2} is targeted through the BUB-1 LxxIxE motif (Figure 6A). Furthermore, B56γ^{PPTR-2} regulation differs from that of B56α^{PPTR-1} in that its localisation also requires an intact BUB-1 kinase domain. This LxxIxE motif-independent pathway could be indirect as the kinase domain of *C. elegans* BUB-1 serves as a platform for different protein-protein interactions (Figure 6A). Importantly, this also explains why the BUB-1 LxxIxE motif mutant has a milder effect than BUB-1 or PPTR-1/2 depletion.

What are the PP2A:B56 meiotic substrates? Human Bub1 phosphorylation in threonine 461, which is important for MAD1 interaction, is counteracted by BubR1-targeted PP2A:B56 in human cultured cells, independent of microtubule-kinetochore interactions (Qian et al., 2017). It will be worth investigating whether PP2A:B56 can regulate BUB-1 phosphorylation levels during *C. elegans* meiosis. This would generate a negative feed-back mechanism whereby BUB-1 targets PP2A:B56, which in turn dephosphorylates BUB-1. Many questions would arise from this observation, such as i) is PP2A:B56 recruitment by BUB-1

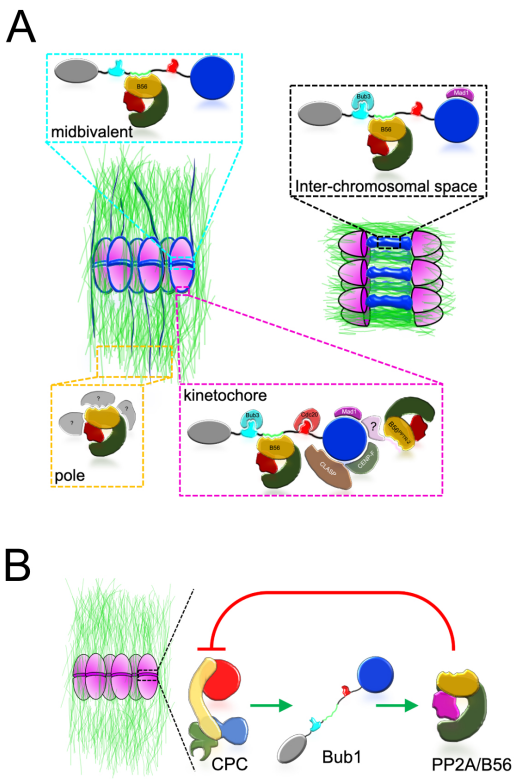

Fig. 6. Summary and hypothesis A. Schematic summary of the different locations of PP2A:B56 and their targeting protein. See Discussion. **B.** Hypothesis for the role for PP2A:B56 in the midbivalent in balancing Aurora B^{AIR-2} kinase activity, allowing for proper chromosome segregation . See Discussion for details.

phospho-regulated? If so, ii) what are the kinases involved? In the case of human Bub1, phosphorylation is achieved by CDK-primed MPS1 phosphorylation (Qian et al., 2017). While nematodes lack an MPS1 orthologue, its function in spindle assembly checkpoint is achieved by PLK-1 (Espeut et al., 2015), making it a likely kinase to perform this putative function.

What is the function of PP2A in the midbivalent? Phosphatase activity is required to balance kinase activity to achieve spatial and temporal regulation of phosphorylation levels. PP2A:B56 counterbalances Aurora B activity in mouse oocytes (Yoshida et al., 2015; Keating et al., 2020). During meiosis in *C. elegans*, the Aurora B orthologue, AIR-2, concentrates in the interface between homologous chromosomes (i.e. the midbivalent (Schumacher et al., 1998; Kaitna et al., 2002; Rogers et al., 2002). Balancing of AIR-2 activity has been reported for PP1, which is recruited during meiosis by the protein LAB-1 (Tzur et al., 2012) and counteracts Aurora B^{AIR-2} during meiosis by antagonising Haspin-mediated H3 T3 phosphorylation in the long arm of the bivalent (where sister chromatid cohesion occurs) (Ferrandiz et al., 2018). Consistent with this, PP1 depletion leads to loss of sister chromatid cohesion during meiosis I (Kaitna et al., 2002; Rogers et al., 2002). As meiosis progresses to the segregation steps, Aurora B^{AIR-2} is present exclusively in the midbivalent and it is therefore expected that its activity will be controlled between the homologues as well, where phosphorylation levels are high (Kitagawa and Rose, 1999; Muscat et al., 2015; Pelisch et al., 2017). However, PP1 is unlikely to achieve this as it resides mainly in kinetochores during meiosis I (Hattersley et al., 2016). Since PP2A:B56 is strongly concentrated in the midbivalent during meiosis I, we hypothesise that it could be the phosphatase balancing AIR-2 activity during meiosis (Figure 6B). It will be interesting to find substrates for Aurora B and PP2A and to test how midbivalent phosphorylation levels during meiosis I are affected by altering the balance between Aurora B and PP2A. In this respect, it was recently shown that B-type subunits affect the dephosphorylation site preference of the PP2A catalytic subunit (Kruse et al., 2020), while we found that serine 612 in BUB-1 is phosphorylated (data not shown). This serine is embedded in a sequence (RRLSI) closely resembling the consensus reported in (Kruse et al., 2020). Interestingly, the sequence also fits into the loosely defined Aurora B consensus RRxSψ (where ψ is a hydrophobic aa) (Cheeseman et al., 2002; Kettenbach et al., 2011; Deretic et al., 2019).

In summary, we provide evidence for a novel, BUB-1-regulated role for PP2A:B56 during female meiosis in *C. elegans*. It will be interesting to test in the future our hypothesis that PP2A is the main phosphatase counteracting Aurora B-mediated phosphorylation to achieve proper phosphorylation levels during meiosis I.

Methods

***C. elegans* strains.** Strains used in this study were maintained at 20 degrees unless indicated otherwise. For a complete list of strains, please refer to Supplementary Table 1. Requests for strains not deposited in the CGC should be done through the FP lab's website (https://pelischlab.co.uk/reagents/).

CRISPR strains. See Supplementary Methods.

Live imaging of oocytes. A detailed protocol for live imaging of *C. elegans* oocytes was used with minor modifications (Laband et al., 2018). Fertilized oocytes were dissected and mounted in 5 µl of L-15 blastomere culture medium (0.5 mg/mL Inulin; 25 mM HEPES, pH 7.5 in 60% Leibowitz L-15 medium and 20% heat-Inactivated FBS) on 24×40 mm 1.5 coverslips. Once dissection was performed and early oocytes identified using a stereomicroscope, a circle of Vaseline was laid around the sample, and a custom-made 24x40 mm plastic holder (with a centred window) was placed on top. The sample was imaged immediately. Live imaging was done using a 60X/NA 1.4 oil objective on a spinning disk confocal microscope (MAG Biosystems) mounted on a microscope (IX81; Olympus), an EMCCD Cascade II camera (Photometrics), spinning-disk head (CSU-X1; Yokogawa Electric Corporation). Acquisition parameters were controlled by MetaMorph 7 software (Molecular Devices). Images were acquired every 20 seconds (with the exception of Figures 1B, 3C, and S1A, where a 30-second interval was used). For all live imaging experiments, partial max-intensity projections are presented

in the figures and full max-intensity projections are presented in the supplementary movies. All files were stored, classified, and managed using OMERO (Allan et al., 2012). Figures were prepared using OMERO.figure and assembled using Adobe Illustrator. Representative movies shown in Supplementary material were assembled using custom-made macros in Fiji/ImageJ (Schindelin et al., 2012).

Immunofluorescence. Worms were placed on 4 µl of M9 worm buffer in a poly-D-lysine (Sigma, P1024)-coated slide and a 24x24-cm coverslip was gently laid on top. Once the worms extruded the embryos, slides were placed on a metal block on dry ice for >10 min. The coverslip was then flicked off with a scalpel blade, and the samples were fixed in methanol at 20°C for 30 min. After blocking in PBS buffer plus 3% BSA and 0.1% Triton X-100 (AbDil), samples were incubated overnight at 4°C with anti-BUB-1 (Desai et al., 2003) and anti-tubulin (1/400, clone DM1 Sigma Aldrich) in AbDil. After three washes with PBS plus 0.1% Tween, secondary antibodies were added at 1/1000 (goat anti-mouse and goat anti-rabbit conjugated to Alexa Fluor488, Alexa Fluor594, Thermo Scientific). After two hours at room temperature and three washes with PBS plus 0.1% Tween, embryos were mounted in ProLong Diamond antifade mountant with DAPI (Thermo Scientific).

GFP immunoprecipitation. For GFP immunoprecipitations, we followed a published protocol (Sonneville et al., 2017) with minor modifications (Pelisch et al., 2019). Approximately 1000 worms expressing GFP-tagged endogenous BUB-1 were grown for two generations at 20°C in large 15-cm NGM plates with concentrated HT115 bacteria. Worms were bleached and embryos were laid in new 15-cm NGM plates with concentrated HT115 bacteria. Once >80% of the worm population was at the L3/L4 stage, worms were washed and placed on 15-cm agarose plates containing concentrated HT115 bacteria. After 24 hs, worms were bleached and the embryos were resuspended in a lysis buffer containing 100 mM HEPES-KOH pH 7.9, 50 mM potassium acetate, 10 mM magnesium acetate, 2 mM EDTA, 1X Protease inhibitor ULTRA (Roche), 2X PhosSTOP (Roche), and 1 mM DTT. The solution was added drop-wise to liquid nitrogen to generate beads that were later grinded using a SPEX SamplePrep 6780 Freezer/Mill. After thawing, we added one-quarter volume of buffer containing lysis buffer supplemented with 50% glycerol, 300 mM potassium acetate, 0.5% NP40, plus DTT, protease and phosphatase inhibitors as above. DNA was digested with 1,600U of Pierce Universal Nuclease for 30 min on ice. Extracts were centrifuged at 25,000 g for 30 min and then at 100,000 g for 1 h. The extract was then incubated for 60 min with 30 µl of a GFP nanobody covalently coupled to magnetic beads. The beads were washed ten times with 1 ml of wash buffer (100 mM HEPES-KOH pH 7.9, 300 mM potassium acetate, 10 mM magnesium acetate, 2 mM EDTA, 0.1% NP40, plus protease and phosphatase inhibitors) at 4°C (cold room). Bound proteins were eluted twice using two rounds of 50 µl LDS sample buffer (Thermo Scientific) at 70°C for 15 min and stored at 80°C.

Sample preparation for mass spectrometry. IP samples were run onm 4-12% Bis-Tris SDS gels with MOPS running buffer and the gel was stained using Quick Coomassie Stain (Generon). Bands of interest were cut and washed with water:acetonitrile (50:50), followed by a wash with 100 mM ammonium bicarbonate. The gel pieces were then washed with 100 mM ammonium bicarbonate:acetonitrile (50:50), followed by a final wash with acetonitrile. Gel pieces were dried using a SpeedVac. Samples were reduced with 10mM DTT in 20 mM ammonium bicarbonate and alkilated With 50 mM IAA in 20 mM ammonium bicarbonate. Samples were then washed sequentially with 100 mM ammonium bicarbonate, 100 mM ammonium bicarbonate:Acetonitrile (50:50), and acetonitrile. Gel pieces were dried using a SpeedVac. Trypsin solution (12.5 µg/ml stock in 20 mM ammonium bicarbonate) was added to cover the gel pieces and and incubated for 30 mins on a shaking platform and incubated sample overnight at 30C on a shaker. Peptides were extracted by standard procedures and reconstituted in 10 µl of 5% formic acid/10% acetonitrile. After vortexing for 1 min, water was added to 50 µl.

Mass Spectrometry analysis. Samples were run on an Ultimate 3000 RSLCnano system (ThermoFisher Scientific) coupled to a Q-Exactive Plus Mass Spectrometer (Thermo Fisher Scientific). Peptides initially trapped on an Acclaim PepMap 100 (Thermo Fisher Scientific) and then separated on an Easy-Spray PepMap RSLC C18 column (Thermo Fisher Scientific). Sample was transferred to mass spectrometer via an Easy-Spray source with temperature set at 50C and a source voltage of 2.1 kV. The mass spectrometer was operated on in data dependent acquisition mode (top 15 method). MS resolution was 70,000 with a mass range of 350 to 1600. MS/MS resolution was 17,500. .RAW data files were extracted and converted to mascot generic files (.mgf) using MSC Convert. Extracted data then searched against Caenorhabditis elegans proteome and BUB-1 specifically, using the Mascot Search Engine (Mascot Daemon Version 2.3.2). Type of search used was MS/MS Ion Search, using Trypsin/P. Carbamidomethyl (C) was set as a fixed modification and variable modifications were as follows: acetyl (N-term), dioxidation (M), Gln to pyro-Glu (N-term Q), Oxidation (M), Deamidation (NQ), and Phosphorylation (STY). Peptide Mass Tolerance was ± 10 ppm (13C = 2) with a Fragment Mass Tolerance of ± 0.6 Da. Maximum number of missed cleavages was 2.

Sequence Alignment. All sequence alignments were performed using Clustal Omega (Sievers et al., 2011), version 1.2.4. Full-length mammalian B56α (UniProtKB Q15172), β (UniProtKB Q15173), γ (UniProtKB Q13362), δ (UniProtKB Q14738) and ϵ (UniProtKB Q16537) alongside their alternative splicing isoforms were retrieved from UniProt (Bateman et.al., 2017) and aligned with full-length *C. elegans* PPTR-1 (UniProtKB O18178) and PPTR-2 (UniProtKB A9UJN4-1). A guide tree was calculated from

the distance matrix generated from sequence pairwise scores.

The C-terminal regions of mammalian isoforms B56γ (S378-A393), δ (S454-A469), β (S409-V424), α (S403-V418), ϵ (S395-V410) and *C. elegans* PPTR-1 (S420-V435) and PPTR-2 (S449-A464) were used for the alignment. The canonical sequences of each B56 isoform were retrieved from UniProt (UniProt, 2019).

The short linear motifs (SLiMs) of *C. elegans* BUB-1 (R279-D292;UniProtKB Q21776), human BubR1 (I666-A679;UniProtKB O60566-1) and RepoMan (K587-P600; UniProtKB Q69YH5-1) were aligned with Clustal Omega (Sievers et al., 2011) and visualised with Jalview (Waterhouse et al., 2009).

Image analysis and Statistics. For time-dependent analysis, metaphase I was taken as time = 0 seconds. This frame was chosen as the previous frame where the first indication of chromosome separation was visible. All image analysis was done in Fiji (Schindelin et al., 2012). For total intensity measurements within the meiotic spindle, images were thresholded and binary images were generated using the ReinyEntropy method and used to automatically generate the regions of interest (ROIs) for each slice (z) and time point (t) or in the sum-projected image. Going through all the slices was particularly necessary when measuring protein intensity associated with a specific structure/location, since the angle of the spindle can lead to erroneous analysis. All ROIs were recorded and, in order to get background measurements, the ROIs were automatically placed on a different oocyte region, away from the spindle. Background-substracted intensity values were then normalised to the maximum intensity value of the control movie using Graphpad Prism 7.0 and are presented as mean $\pm$ s.e.m.

Central spindle to chromosome ratio for PPTR-2::GFP (Figure 4G) were obtained as follows. Images were selected at early anaphase (t = 40 sec) and to obtain the chromosome ROIs, we used the mCherry::histone channel to create a mask. These ROIs were transferred to the PPTR-2::GFP channel and the intensity was measured as above. The region between the chromosomes was selected intensities were measured to obtain the central spindle intensity. Background corrected values were used to obtain the ratio central spindle/chromosome. Results are shown as median with interquartile range and differences were analysed using an unpaired two-tailed t-test with Welch's correction.

Contingency tables were analysed using the Fisher's exact test (two-tailed) and the P values are presented in the figures and/or in the text.

Generation of Supplementary movies. The 4D TIFF files were converted to movie (.avi) files using a custom-made macro that uses the StackReg Fiji plugin for image registration. Movies were assembled using max intensity projections hence the movies might not match a specific panel within the main figures, which are single slices or partial projections in order to highlight specific characteristics.

ACKNOWLEDGEMENTS

We would like to thank Guy Benian, Needhi Bhalla, Bruce Bowerman, Arshad Desai, and Tony Hyman for sharing C. elegans strains and antibodies. We would like to thank Egon Ogris for sharing unpublished data on the use of the PP2Ac monoclonal antibody. We thank Arshad Desai, Ron Hay, and Tomo Tanaka for comments on the manuscript. This work was supported by a Career Development Award from the Medical Research Council (grant MR/R008574/1) and an ISSF grant funded by the Wellcome Trust (105606/Z/14/Z). ST is funded by a Medical Research Council Doctoral Training Programme. D.K.C. is supported by a Sir Henry Dale Fellowship from the Wellcome Trust (208833). P.L-G. and J.B. were supported by NIH grant R01 GM074215, awarded to Arshad Desai. Work in the J.N.B. lab is supported by NIH grant R01 GM114471. We acknowledge the FingerPrints Proteomics Facility and the Dundee Imaging Facility, which are supported by a 'Wellcome Trust Technology Platform' award (097945/B/11/Z) and the Tissue Imaging Facility, funded by a Wellcome Trust award (101468/Z/13/Z). Some nematode strains were provided by the CGC, which is funded by NIH Office of Research Infrastructure Programs (P40 OD010440).

References

Allan, C., Burel, J.M., Moore, J., Blackburn, C., Linkert, M., Loynton, S., Macdonald, D., Moore, W.J., Neves, C., Patterson, A., Porter, M., Tarkowska, A., Loranger, B., Avondo, J., Lagerstedt, I., Lianas, L., Leo, S., Hands, K., Hay, R.T., Patwardhan, A., Best, C., Kleywegt, G.J., Zanetti, G., and Swedlow, J.R. (2012). OMERO: flexible, model-driven data management for experimental biology. Nat Methods 9, 245-253.

Cheeseman, I.M., Anderson, S., Jwa, M., Green, E.M., Kang, J., Yates, J.R., 3rd, Chan, C.S., Drubin, D.G., and Barnes, G. (2002). Phospho-regulation of kinetochore-microtubule attachments by the Aurora kinase Ipl1p. Cell 111, 163-172.

Cho, U.S., and Xu, W. (2007). Crystal structure of a protein phosphatase 2A heterotrimeric holoenzyme. Nature 445, 53-57.

de Carvalho, C.E., Zaaijer, S., Smolikov, S., Gu, Y., Schumacher, J.M., and Colaiacovo, M.P. (2008). LAB-1 antagonizes the Aurora B kinase in C. elegans. Genes Dev 22, 2869-2885.

Deretic, J., Kerr, A., and Welburn, J.P.I. (2019). A rapid computational approach identifies SPICE1 as an Aurora kinase substrate. Mol Biol Cell 30, 312-323.

Desai, A., Rybina, S., Müller-Reichert, T., Shevchenko, A., Shevchenko, A., Hyman, A., and Oegema, K. (2003). KNL-1 directs assembly of the microtubule-binding interface of the kinetochore in C. elegans. Genes Development 17, 2421-2435.

Dickinson, D.J., Pani, A.M., Heppert, J.K., Higgins, C.D., and Goldstein, B. (2015). Streamlined Genome Engineering with a Self-Excising Drug Selection Cassette. Genetics 200, 1035-1049.

Dumont, J., Oegema, K., and Desai, A. (2010). A kinetochore-independent mechanism drives anaphase chro-

mosome separation during acentrosomal meiosis. Nat Cell Biol 12, 894-901.

Elowe, S. (2011). Bub1 and BubR1: at the interface between chromosome attachment and the spindle checkpoint. Mol Cell Biol 31, 3085-3093.

Espert, A., Uluocak, P., Bastos, R.N., Mangat, D., Graab, P., and Gruneberg, U. (2014). PP2A-B56 opposes Mps1 phosphorylation of Knl1 and thereby promotes spindle assembly checkpoint silencing. The Journal of Cell Biology 206, 833.

Essex, A., Dammermann, A., Lewellyn, L., Oegema, K., and Desai, A. (2009). Systematic analysis in Caenorhabditis elegans reveals that the spindle checkpoint is composed of two largely independent branches. Mol Biol Cell 20, 1252-1267.

Ferrandiz, N., Barroso, C., Telecan, O., Shao, N., Kim, H.-M., Testori, S., Faull, P., Cutillas, P., Snijders, A.P., Colaiácovo, M.P., and Martinez-Perez, E. (2018). Spatiotemporal regulation of Aurora B recruitment ensures release of cohesion during C. elegans oocyte meiosis. Nature Communications 9, 834.

Foley, E.A., Maldonado, M., and Kapoor, T.M. (2011). Formation of stable attachments between kinetochores and microtubules depends on the B56-PP2A phosphatase. Nature Cell Biology 13, 1265-1271.

Gelens, L., Qian, J., Bollen, M., and Saurin, A.T. (2018). The Importance of Kinase-Phosphatase Integration: Lessons from Mitosis. Trends Cell Biol 28, 6-21.

Hassold, T., and Hunt, P. (2001). To err (meiotically) is human: the genesis of human aneuploidy. Nat Rev Genet 2, 280-291.

Hattersley, N., Cheerambathur, D., Moyle, M., Stefanutti, M., Richardson, A., Lee, K.Y., Dumont, J., Oegema, K., and Desai, A. (2016). A Nucleoporin Docks Protein Phosphatase 1 to Direct Meiotic Chromosome Segregation and Nuclear Assembly. Dev Cell 38, 463-477.

Hayward, D., Bancroft, J., Mangat, D., Alfonso-Pérez, T., Dugdale, S., McCarthy, J., Barr, F.A., and Gruneberg, U. (2019). Checkpoint signaling and error correction require regulation of the MPS1 T-loop by PP2A-B56. The Journal of Cell Biology, jcb.201905026.

Hertz, E.P.T., Kruse, T., Davey, N.E., Lopez-Mendez, B., Sigurethsson, J.O., Montoya, G., Olsen, J.V., and Nilsson, J. (2016). A Conserved Motif Provides Binding Specificity to the PP2A-B56 Phosphatase. Molecular Cell 63, 686-695.

Homer, H., Gui, L., and Carroll, J. (2009). A spindle assembly checkpoint protein functions in prophase I arrest and prometaphase progression. Science 326, 991-994.

Kaitna, S., Pasierbek, P., Jantsch, M., Loidl, J., and Glotzer, M. (2002). The aurora B kinase AIR-2 regulates kinetochores during mitosis and is required for separation of homologous Chromosomes during meiosis. Curr Biol 12, 798-812.

Keating, L., Touati, S.A., and Wassmann, K. (2020). A PP2A-B56-Centered View on Metaphase-to-Anaphase Transition in Mouse Oocyte Meiosis I. Cells 9.

Kettenbach, A.N., Schweppe, D.K., Faherty, B.K., Pechenick, D., Pletnev, A.A., and Gerber, S.A. (2011). Quantitative phosphoproteomics identifies substrates and functional modules of Aurora and Polo-like kinase activities in mitotic cells. Sci Signal 4, rs5.

Kim, T., Lara-Gonzalez, P., Prevo, B., Meitinger, F., Cheerambathur, D.K., Oegema, K., and Desai, A. (2017). Kinetochores accelerate or delay APC/C activation by directing Cdc20 to opposing fates. Genes Dev 31, 1089-1094.

Kim, T., Moyle, M.W., Lara-Gonzalez, P., De Groot, C., Oegema, K., and Desai, A. (2015). Kinetochore-localized BUB-1/BUB-3 complex promotes anaphase onset in C. elegans. J Cell Biol 209, 507-517.

Kitagawa, D., Fluckiger, I., Polanowska, J., Keller, D., Reboul, J., and Gonczy, P. (2011). PP2A phosphatase acts upon SAS-5 to ensure centriole formation in C. elegans embryos. Dev Cell 20, 550-562.

Kitagawa, R., and Rose, A.M. (1999). Components of the spindle-assembly checkpoint are essential in Caenorhabditis elegans. Nat Cell Biol 1, 514-521.

Kitajima, T.S., Sakuno, T., Ishiguro, K.-i., Iemura, S.-i., Natsume, T., Kawashima, S.A., and Watanabe, Y. (2006). Shugoshin collaborates with protein phosphatase 2A to protect cohesin. Nature 441, 46-52.

Kruse, T., Gnosa, S.P., Nasa, I., Garvanska, D.H., Hein, J.B., Nguyen, H., Samsoe-Petersen, J., Lopez-Mendez, B., Hertz, E.P.T., Schwarz, J., Pena, H.S., Nikodemus, D., Kveiborg, M., Kettenbach, A.N., and Nilsson, J. (2020). Mechanisms of site-specific dephosphorylation and kinase opposition imposed by PP2A regulatory subunits. EMBO J, e103695.

Kruse, T., Zhang, G., Larsen, M.S., Lischetti, T., Streicher, W., Kragh Nielsen, T., Bjorn, S.P., and Nilsson, J. (2013). Direct binding between BubR1 and B56-PP2A phosphatase complexes regulate mitotic progression. Journal of Cell Science 126, 1086-1092.

Laband, K., Lacroix, B., Edwards, F., Canman, J.C., and

Dumont, J. (2018). Methods in Cell Biology, Vol 145.

Laband, K., Le Borgne, R., Edwards, F., Stefanutti, M., Canman, J.C., Verbavatz, J.M., and Dumont, J. (2017). Chromosome segregation occurs by microtubule pushing in oocytes. Nat Commun 8, 1499. Lange, K.I., Heinrichs, J., Cheung, K., and Srayko, M. (2013). Suppressor mutations identify amino acids in PAA-1/PR65 that facilitate regulatory RSA-1/B subunit targeting of PP2A to centrosomes in C. elegans. Biology open 2, 88-94.

Magescas, J., Zonka, J.C., and Feldman, J.L. (2019). A two-step mechanism for the inactivation of microtubule organizing center function at the centrosome. eLife 8, e47867. Marston, A.L., and Amon, A. (2004). Meiosis: cell-cycle controls shuffle and deal. Nat Rev Mol Cell Biol 5, 983-997.

Monen, J., Maddox, P.S., Hyndman, F., Oegema, K., and Desai, A. (2005). Differential role of CENP-A in the segregation of holocentric C. elegans chromosomes during meiosis and mitosis. Nature Cell Biology 7, 1248.

Moura, M., and Conde, C. (2019). Phosphatases in Mitosis: Roles and Regulation. Biomolecules 9. Moyle, M.W., Kim, T., Hattersley, N., Espeut, J., Cheerambathur, D.K., Oegema, K., and Desai, A. (2014). A Bub1-Mad1 interaction targets the Mad1-Mad2 complex to unattached kinetochores to initiate the spindle checkpoint. J Cell Biol 204, 647-657.

Muscat, C.C., Torre-Santiago, K.M., Tran, M.V., Powers, J.A., and Wignall, S.M. (2015). Kinetochore-independent chromosome segregation driven by lateral microtubule bundles. Elife 4, e06462.

Nilsson, J. (2015). Bub1/BubR1: swiss army knives at kinetochores. Cell Cycle 14, 2999-3000. Novak, B., Kapuy, O., Domingo-Sananes, M.R., and Tyson, J.J. (2010). Regulated protein kinases and phosphatases in cell cycle decisions. Curr Opin Cell Biol 22, 801-808.

Ohkura, H. (2015). Meiosis: an overview of key differences from mitosis. Cold Spring Harb Perspect Biol 7.

Padmanabhan, S., Mukhopadhyay, A., Narasimhan, S.D., Tesz, G., Czech, M.P., and Tissenbaum, H.A. (2009). A PP2A regulatory subunit regulates C. elegans insulin/IGF-1 signaling by modulating AKT-1 phosphorylation. Cell 136, 939-951.

Pal, S., Lant, B., Yu, B., Tian, R., Tong, J., Krieger, J.R., Moran, M.F., Gingras, A.C., and Derry, W.B. (2017). CCM-3 Promotes C. elegans Germline Development by Regulating Vesicle Trafficking Cytokinesis and Polarity. Curr Biol 27, 868-876.

Pelisch, F., Bel Borja, L., Jaffray, E.G., and Hay, R.T. (2019). Sumoylation regulates protein dynamics during meiotic chromosome segregation in C. elegans oocytes. Journal of Cell Science 132, jcs232330.

Pelisch, F., Tammsalu, T., Wang, B., Jaffray, E.G., Gartner, A., and Hay, R.T. (2017). A SUMO-Dependent Protein Network Regulates Chromosome Congression during Oocyte Meiosis. Mol Cell 65, 66-77.

Qian, J., Garcia-Gimeno, M.A., Beullens, M., Manzione, M.G., Van der Hoeven, G., Igual, J.C., Heredia, M., Sanz, P., Gelens, L., and Bollen, M. (2017). An Attachment-Independent Biochemical Timer of the Spindle Assembly Checkpoint. Mol Cell 68, 715-730 e715.

Riedel, C.G., Katis, V.L., Katou, Y., Mori, S., Itoh, T., Helmhart, W., Gálová, M., Petronczki, M., Gregan, J., Cetin, B., Mudrak, I., Ogris, E., Mechtler, K., Pelletier, L., Buchholz, F., Shirahige, K., and Nasmyth, K. (2006). Protein phosphatase 2A protects centromeric sister chromatid cohesion during meiosis I. Nature 441, 53-61.

Rogers, E., Bishop, J.D., Waddle, J.A., Schumacher, J.M., and Lin, R. (2002). The aurora kinase AIR-2 functions in the release of chromosome cohesion in Caenorhabditis elegans meiosis. J Cell Biol 157, 219-229.

Schindelin, J., Arganda-Carreras, I., Frise, E., Kaynig, V., Longair, M., Pietzsch, T., Preibisch, S., Rueden, C., Saalfeld, S., Schmid, B., Tinevez, J.Y., White, D.J., Hartenstein, V., Eliceiri, K., Tomancak, P., and Cardona, A. (2012). Fiji: an open-source platform for biological-image analysis. Nat Methods 9, 676-682.

Schlaitz, A.-L., Srayko, M., Dammermann, A., Quintin, S., Wielsch, N., MacLeod, I., de Robillard, Q., Zinke, A., Yates, J.R., Müller-Reichert, T., Shevchenko, A., Oegema, K., and Hyman, A.A. (2007). The C. elegans RSA Complex Localizes Protein Phosphatase 2A to Centrosomes and Regulates Mitotic Spindle Assembly. Cell 128, 115-127.

Schumacher, J.M., Golden, A., and Donovan, P.J. (1998). AIR-2: An Aurora/Ipl1-related protein kinase associated with chromosomes and midbody microtubules is required for polar body extrusion and cytokinesis in Caenorhabditis elegans embryos. J Cell Biol 143, 1635-1646.

Seshacharyulu, P., Pandey, P., Datta, K., and Batra, S.K. (2013). Phosphatase: PP2A structural importance, regulation and its aberrant expression in cancer. Cancer Letters 335, 9-18.

Shi, Y. (2009). Serine/threonine phosphatases: mechanism through structure. Cell 139, 468-484.

Sieburth, D.S., Sundaram, M., Howard, R.M., and Han, M. (1999). A PP2A regulatory subunit positively regulates

Ras-mediated signaling during Caenorhabditis elegans vulval induction. Genes Dev 13, 2562-2569.

Sievers, F., Wilm, A., Dineen, D., Gibson, T.J., Karplus, K., Li, W., Lopez, R., McWilliam, H., Remmert, M., Soding, J., Thompson, J.D., and Higgins, D.G. (2011). Fast, scalable generation of high-quality protein multiple sequence alignments using Clustal Omega. Mol Syst Biol 7, 539.

Song, M.H., Liu, Y., Anderson, D.E., Jahng, W.J., and O'Connell, K.F. (2011). Protein phosphatase 2A-SUR-6/B55 regulates centriole duplication in C. elegans by controlling the levels of centriole assembly factors. Dev Cell 20, 563-571.

Suijkerbuijk, S.J., Vleugel, M., Teixeira, A., and Kops, G.J. (2012). Integration of kinase and phosphatase activities by BUBR1 ensures formation of stable kinetochore-microtubule attachments. Dev Cell 23, 745-755.

Tang, Z., Shu, H., Qi, W., Mahmood, N.A., Mumby, M.C., and Yu, H. (2006). PP2A Is Required for Centromeric Localization of Sgo1 and Proper Chromosome Segregation. Developmental Cell 10, 575-585. Touati, S.A., Buffin, E., Cladiere, D., Hached, K., Rachez, C., van Deursen, J.M., and Wassmann, K. (2015). Mouse oocytes depend on BubR1 for proper chromosome segregation but not for prophase I arrest. Nat Commun 6, 6946.

Tzur, Y.B., Egydio de Carvalho, C., Nadarajan, S., Van Bostelen, I., Gu, Y., Chu, D.S., Cheeseman, I.M., and Colaiacovo, M.P. (2012). LAB-1 targets PP1 and restricts Aurora B kinase upon entrance into meiosis to promote sister chromatid cohesion. PLoS Biol 10, e1001378.

UniProt, C. (2019). UniProt: a worldwide hub of protein knowledge. Nucleic Acids Res 47, D506-D515. Vallardi, G., Allan, L.A., Crozier, L., and Saurin, A.T. (2019). Division of labour between PP2A-B56 isoforms at the centromere and kinetochore. eLife 8, e42619.

Van Roey, K., and Davey, N.E. (2015). Motif co-regulation and co-operativity are common mechanisms in transcriptional, post-transcriptional and post-translational regulation. Cell Communication and Signaling 13, 45.

Wang, S., Wu, D., Quintin, S., Green, R.A., Cheerambathur, D.K., Ochoa, S.D., Desai, A., and Oegema, K. (2015). NOCA-1 functions with gamma-tubulin and in parallel to Patronin to assemble non-centrosomal microtubule arrays in C. elegans. Elife 4, e08649.

Wang, X., Bajaj, R., Bollen, M., Peti, W., and Page, R. (2016). Expanding the PP2A Interactome by Defining a B56-Specific SLiM. Structure 24, 2174-2181.

Waterhouse, A.M., Procter, J.B., Martin, D.M., Clamp, M., and Barton, G.J. (2009). Jalview Version 2–a multiple sequence alignment editor and analysis workbench. Bioinformatics 25, 1189-1191.

Xu, P., Raetz, E.A., Kitagawa, M., Virshup, D.M., and Lee, S.H. (2013). BUBR1 recruits PP2A via the B56 family of targeting subunits to promote chromosome congression. Biology Open 2, 479.

Xu, P., Virshup, D.M., and Lee, S.H. (2014). B56-PP2A regulates motor dynamics for mitotic chromosome alignment. Journal of Cell Science 127, 4567.

Xu, Y., Chen, Y., Zhang, P., Jeffrey, P.D., and Shi, Y. (2008). Structure of a Protein Phosphatase 2A Holoenzyme: Insights into B55-Mediated Tau Dephosphorylation. Molecular Cell 31, 873-885.

Xu, Y., Xing, Y., Chen, Y., Chao, Y., Lin, Z., Fan, E., Yu, J.W., Strack, S., Jeffrey, P.D., and Shi, Y. (2006). Structure of the Protein Phosphatase 2A Holoenzyme. Cell 127, 1239-1251.

Xu, Z., Cetin, B., Anger, M., Cho, U.S., Helmhart, W., Nasmyth, K., and Xu, W. (2009). Structure and Function of the PP2A-Shugoshin Interaction. Molecular Cell 35, 426-441.

Yoshida, S., Kaido, M., and Kitajima, T.S. (2015). Inherent Instability of Correct Kinetochore-Microtubule Attachments during Meiosis I in Oocytes. Dev Cell 33, 589-602.

Bel Borja et al. Supp. Figure 1

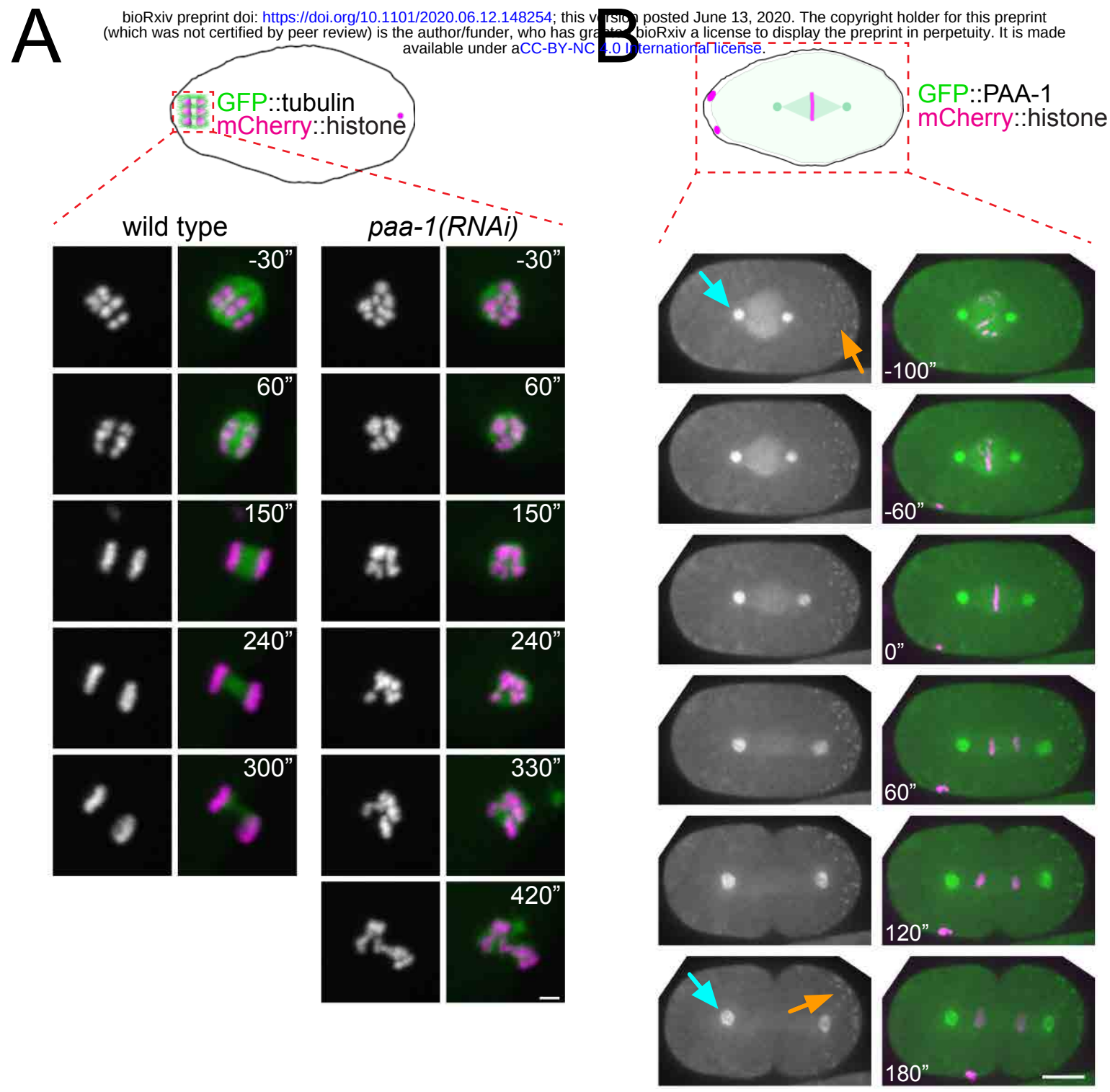

Supplementary Figure 1. PP2A is essential for Meiosis I in *C. elegans* oocytes.

(A) Microtubule and chromosome dynamics were followed in wild type and *paa-1(RNAi)* oocytes expressing GFP::tubulin and mCherry::histone. Inset numbers represent the time relative to metaphase I in seconds. See also Supp. Movie 1. Scale bar, 2 μm.

(B) PAA-1 localisation was followed during the first mitotic division using endogenously tagged GFP::PAA-1. Cyan arrows point to centrosomes and orange arrows point to P-bodies. Inset numbers represent the time relative to metaphase in seconds. Scale bar, 10 μm.

A

Regulatory (B) Subunit	
human	*C. elegans*
PPP2R2A / B55α	SUR-6
PPP2R2B / B55β	
PPP2R2C / B55γ	
PPP2R2D / B55δ	
PPP2R5C / B56γ	PPTR-2
PPP2R5D / B56δ	
PPP2R5A / B56α	PPTR-1
PPP2R5E / B56ε	
PPP2R5B / B56β	

B

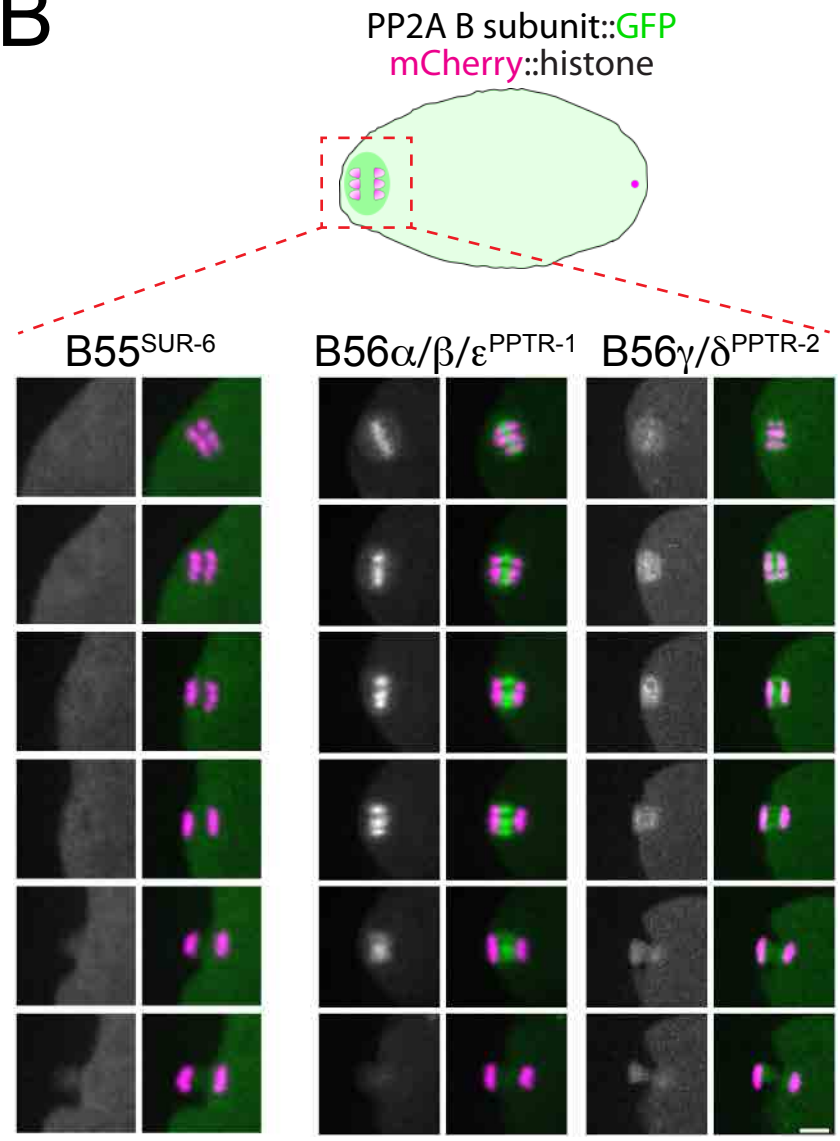

C

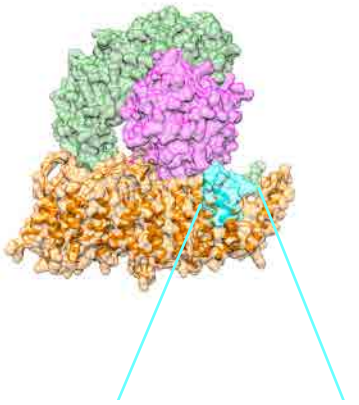

```
B56γ     378- SKTHWNKTIHGLIYNA -393
B56δ     454- SKSHWNKTIHGLIYNA -469
PPTR-2   449- SKSHWNKTIHGLIYNA -464
B56β     409- SKEHWNQTIVSLIYNV -424
PPTR-1   420- SKEHWNQTIVALVYNV -435
B56α     403- SKEHWNPTIVALVYNV -418
B56ε     395- SKEHWNPAIVALVYNV -410
              ** *** :* .*:**.
```

Supplementary Figure 2. Localisation of *C. elegans* B55 and B56 subunits.

(A) Chart showing the C. elegans orthologues of the human B55 and B56 regulatory B subunits. The chart is based on the alignment provided in Table 1 and Supplementary Table 1.

(B) The respective B subunit was endogenously tagged with GFP and their localisation was followed by imaging of dissected oocytes. Scale bar, 2 µm.

(C) Alignment of the human and *C. elegans* B56 subunits in the C-terminal stretch shown to be important for kinetochore vs centromere localisation of B56 in human cells during mitosis (Vallardi et al. 2019).

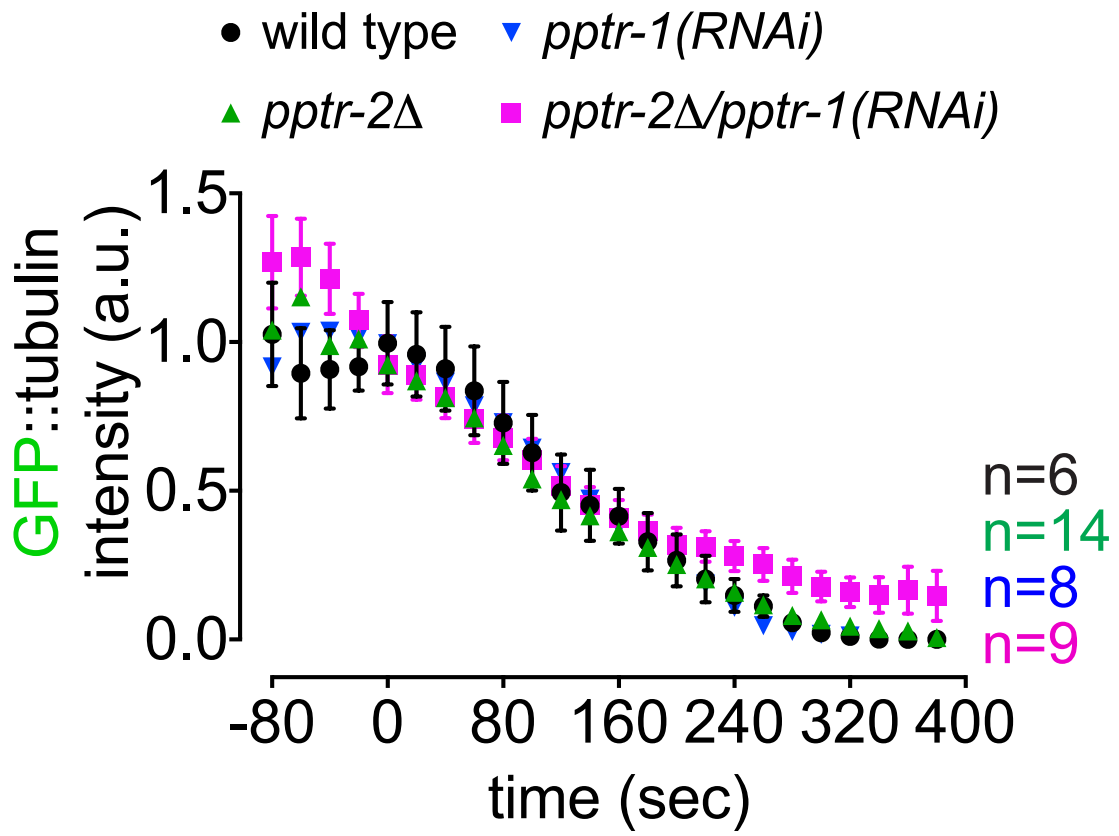
wild type
pptr-1(RNAi)
pptr-2Δ
pptr-2Δ/pptr-1(RNAi)
GFP::tubulin intensity (a.u.)
1.5
1.0
0.5
0.0
-80
0
80
160
240
320
400
time (sec)
n=6
n=14
n=8
n=9

Supplementary Figure 3. GFP::Tubulin levels during meiosis in the absence of PPTR-1/2.

GFP::Tubulin levels were measured in wild type, *pptr-1(RNAi)*, *pptr-2Δ*, and the double PPTR depletion, *pptr2Δ/pptr-1(RNAi)*. Time = 0 corrsponds to metaphase I.

Bel Borja et al. Supp. Figure 4

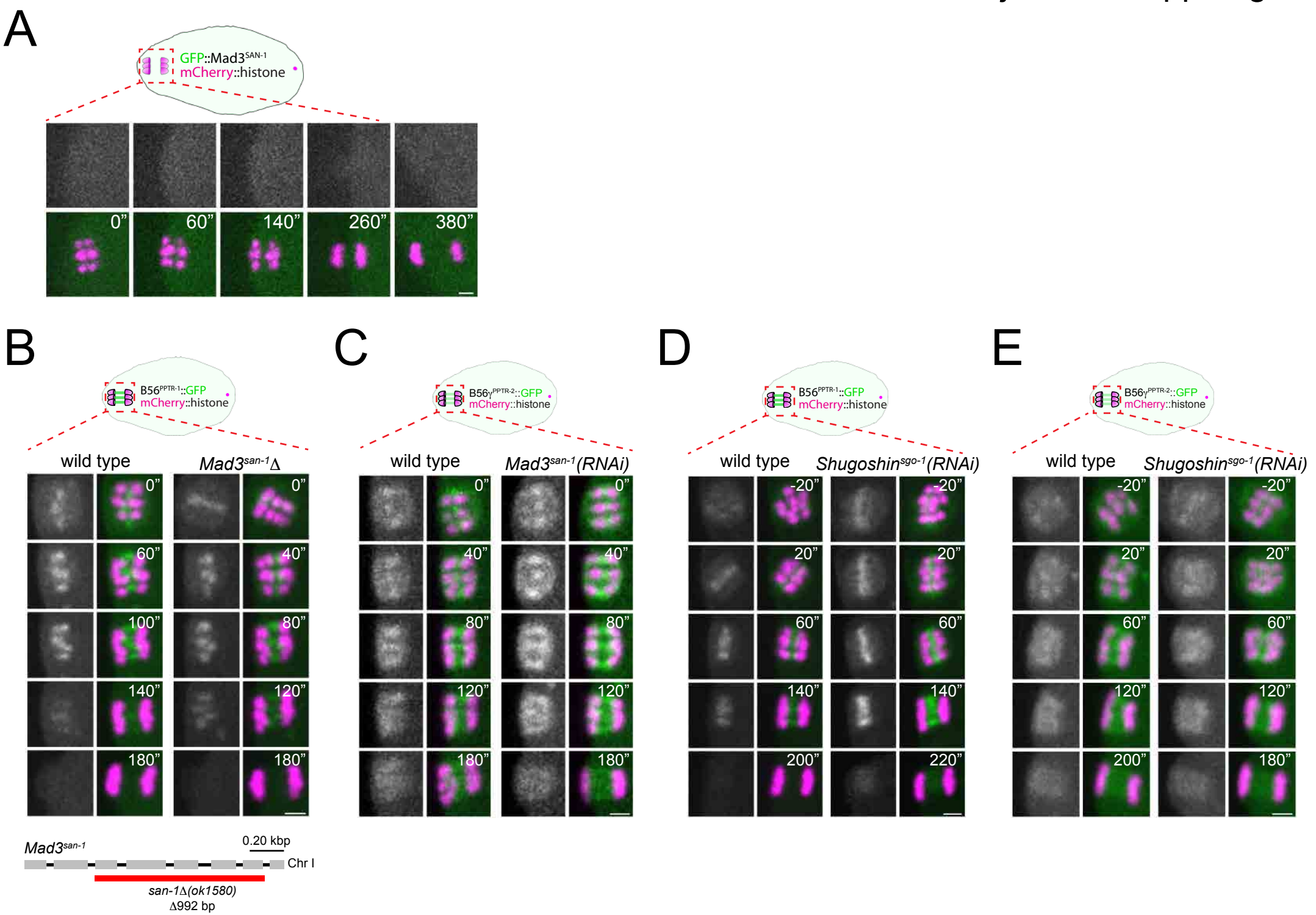

Supplementary Figure 4. Mad3^{SAN-1} and ShugoshinSGO-1 do not play a major role in B56α^{PPTR-1} and B56γ^{PPTR-2} targeting.

(A) GFP::Mad3^{SAN-1} was imaged during oocyte meiosis along with mCherry::histone to follow chromosomes. Time insets are relative to metaphase I (t=0"). Scale bar, 2 µm.

(B) B56α^{PPTR-1} and chromosome dynamics were followed in wild type and in *Mad3^{SAN-1}Δ* oocytes expressing PPTR-1::GFP and mCherry::histone. Scale bar, 2 µm. The bottom panel shows a schematic of the *san-1Δ* allele.

(C) B56γ^{PPTR-2} and chromosome dynamics were followed in wild type and in *Mad3^{san-1}(RNAi)* oocytes expressing PPTR-2::GFP and mCherry::histone. Scale bar, 2 µm. See also Supplementary Movie 7.

(D) B56α^{PPTR-1} and chromosome dynamics were followed in wild type and in *Shugoshin^{sgo-1}(RNAi)* oocytes expressing PPTR-1::GFP and mCherry::histone. Scale bar, 2 µm.

(E) B56γ^{PPTR-2} and chromosome dynamics were followed in wild type and *Shugoshin^{sgo-1}(RNAi)* oocytes expressing PPTR-2::GFP and mCherry::histone. Scale bar, 2 µm. See also Supplementary Movie 8.

Bel Borja et al. Supp. Figure 5

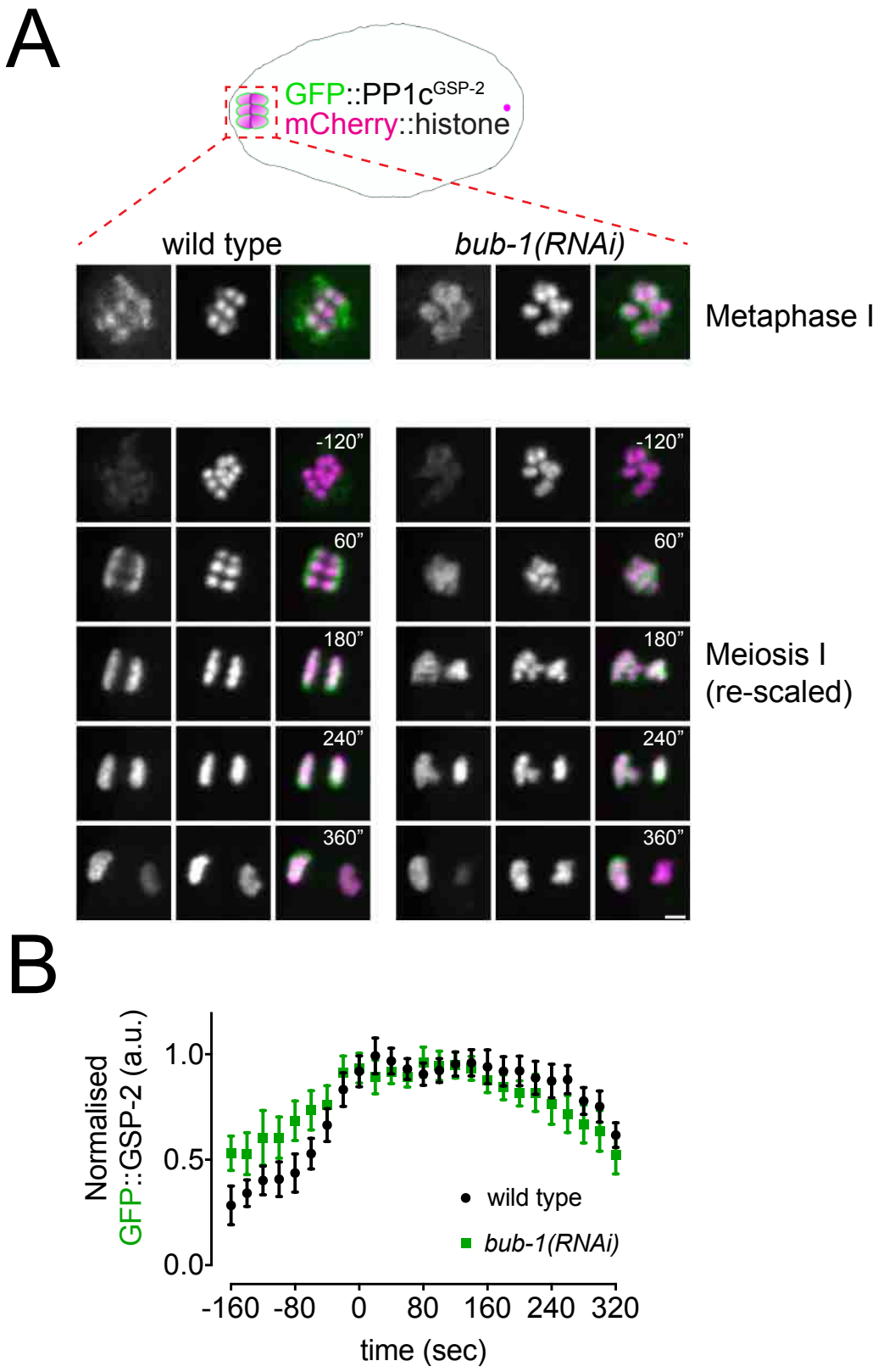

Supplementary Figure 5. PP1 catalytic subunit localisation is not regulated by BUB-1.

(A) GFP::PP1c^{GSP-2} and chromosome dynamics were followed in wild type and *bub-1(RNAi)* oocytes. Since the GFP signal increases during anaphase, one scale was chosen to show kinetochore localisation during metaphase I (top) and another for the composite panel (bottom). Scale bar, 2 µm. See also Supplementary Movie 11.

(B) GFP::PP1c^{GSP-2} levels were measured in wild type and *bub-1(RNAi)* oocytes throughout meiosis I and the mean ± s.e.m is shown in the graph.

Bel Borja et al. Supp. Figure 6

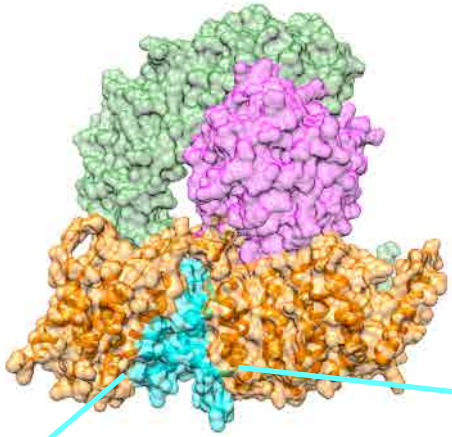

Leu binding pocket

Ile binding pocket

Glu binding pocket

(Wang et al 2016)

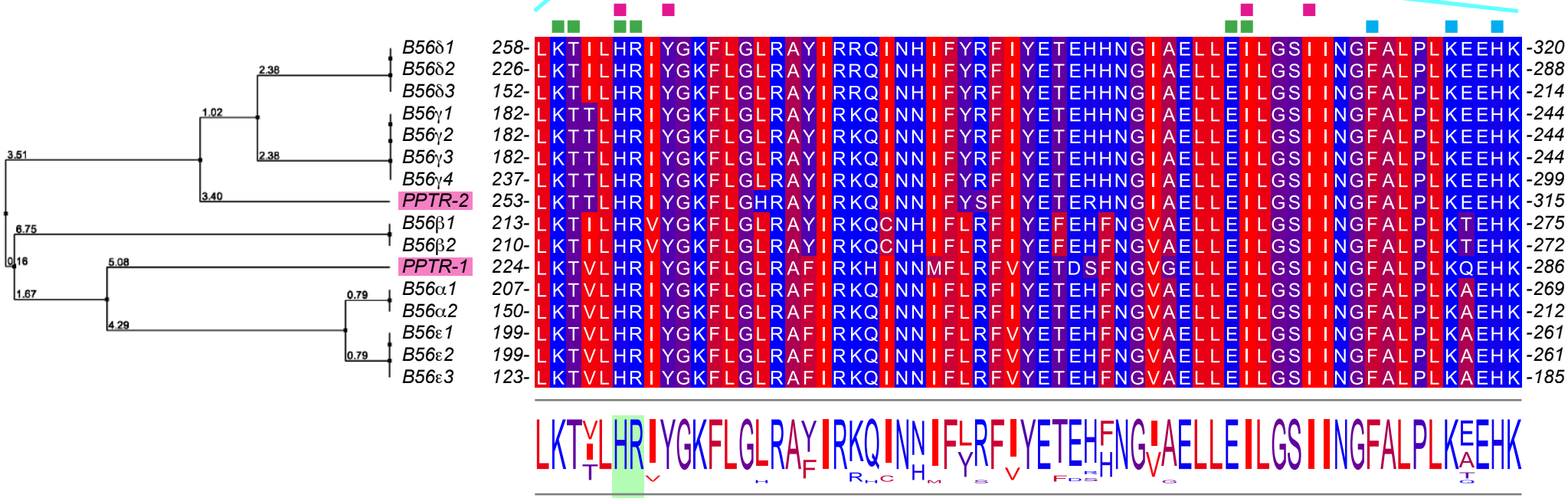

hydrophobic — hydrophilic

R188 (B56γ1) salt bridge with phS (SLiM)

H187 (B56γ1) H-bond with phS carbonyl (SLiM)

Supplementary Figure 6. Alignment of the B56 subunits LxxIxE motif binding pocket.

C. elegans and human B56 subunits LxxIxE motif binding pocket were aligned using Clustal Omega and Jalview. The scale from blue to red represents increasing hydrophobicity. Key residues as reported in Wang et al. (2016) are highlighted. Additionally, residues making contact with the phospho-serine are highlighted with green background. The tree on the left was calculated from the distance matrix generated from sequence pairwise scores and confirms the relationship between *C. elegans* and human B56s.

A

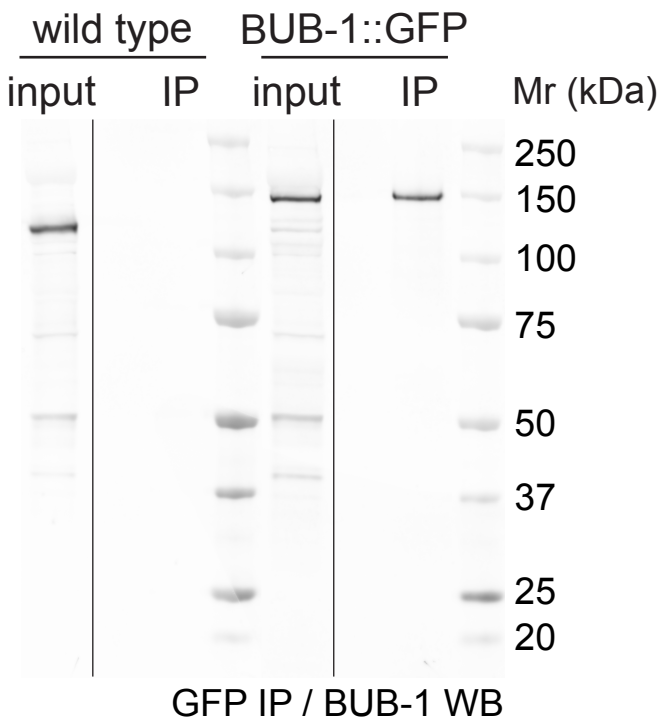

B

R.HLphSPVSEK.T

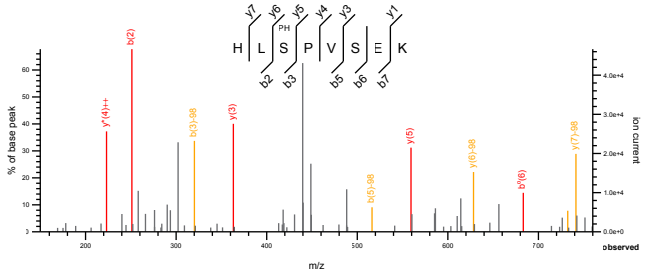

R.RHLphSPVSEK.T

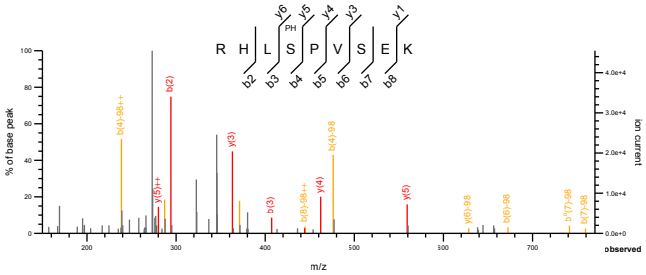

R.RRHLphSPVSEK.T

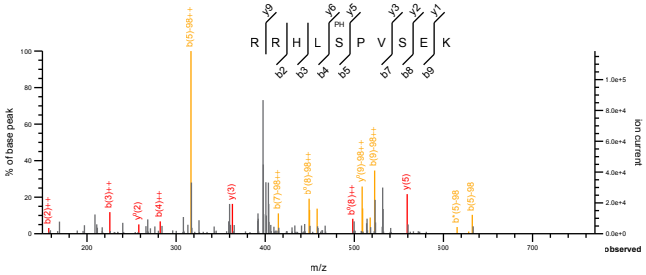

Supplementary Figure 7. BUB-1::GFP immunoprecipitation and selected MS spectra of peptides containing phospho serine 283.

(A) Embryo extracts from wild type (N2) and BUB-1::GFP worms were immunoprecipitated using a GFP nanobody coupled to magnetic beads. The inputs and immunoprecipitates were resolved on SDS-PAGE and subject to BUB-1 western blot. BUB-1::GFP is readily pulled down form the extracts, whereas untagged BUB-1 is not. Note the size difference due to the GFP tag. MW marker is shown on the right side.

(B) Seleted MS spectra without (top), with one (middle), or with two (bottom) trypsin miscleavages are shown.

Bel Borja et al. Supp. Figure 8

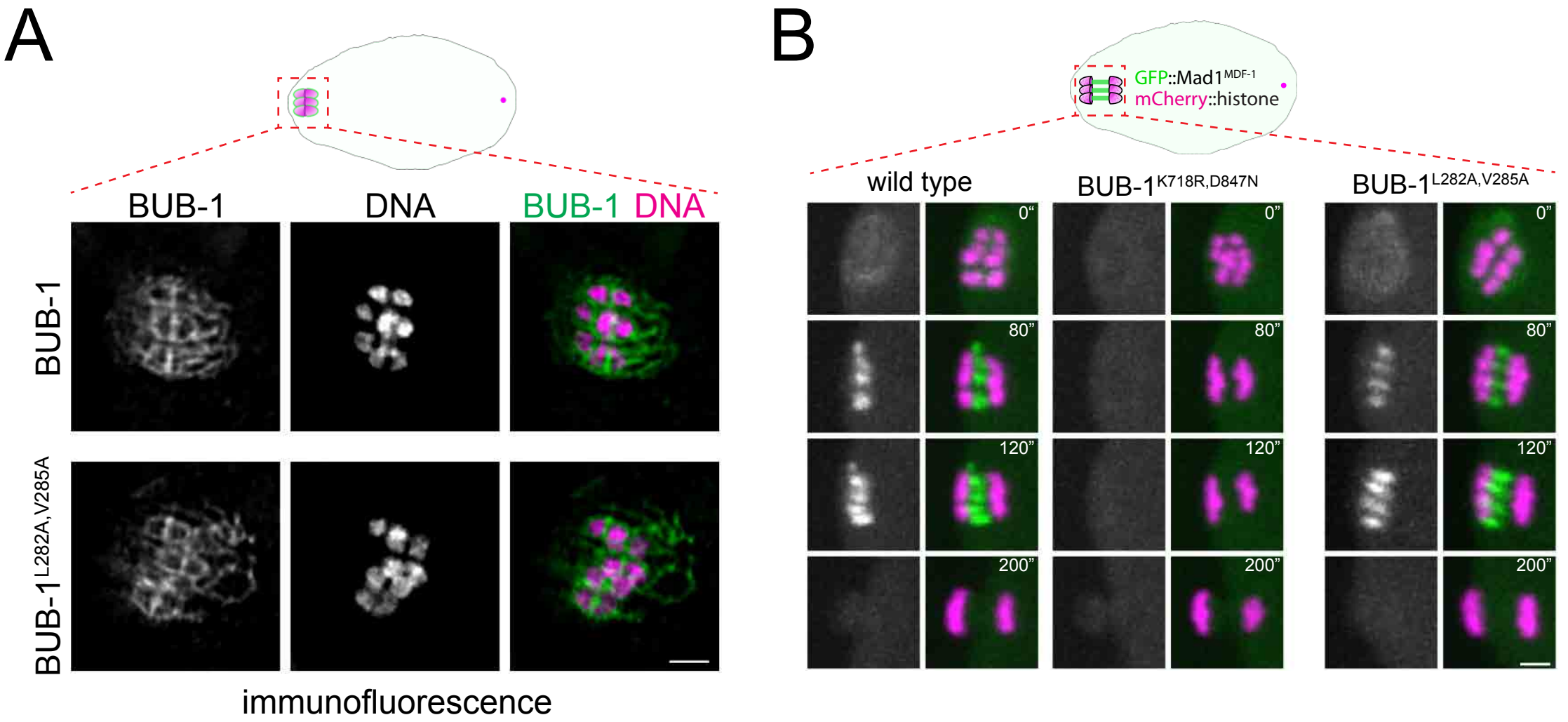

Supplementary Figure 8. Mad1^{MDF-1} localisation is not affected by a LxxIxE motif mutation in BUB-1.

(A) BUB-1 localisation was analysed in fixed wild type and BUB-1^{L282A,V285A} mutant oocytes by immunofluorescence using BUB-1 specific antibodies. Scale bar, 2 µm.

(B) GFP::Mad1^{MDF-1} was imaged during oocyte meiosis along with mCherry::histone to follow chromosomes. Time insets are relative to metaphase I (t=0"). The BUB-1^{K718R,D847N} mutation completely abolishes Mad1^{MDF-1} localisation. On the other hand, GFP::Mad1^{MDF-1} remained unaltered in the the BUB-1^{L282A,V285A} mutant. Scale bar, 2 µm.

Markers / *mutants*	Alelle	Primers (5'-3')	primer name	Restriction enzyme
bub-1(L282A;V285A)	*bub-1(syb1936[bub-1((L282A;V285A)])I*	ATGGAATATCGATTGAGGAGTTTC	fgp_153	*NsiI*
		CAATTTCGGGTTGTACTTCAGA	fgp_154	
bub-1(K718R;D847N)	*bub-1(syb1746[bub-1((K718R;D847N)])I*	GATGTGTCTTGTGCGTCCTC	fgp_125	*BmrI*
		CCAGTCCGGAAGTGAATCA	fgp_126	
pptr-2Δ	*pptr-2(ok1467)V*	ATCCTTGCTAAGCACAGTTGAAGT	fgp_137	
		CGTGAACGTGACTTTCTGAAGA	fgp_138	
san-1Δ	*san-1(ok1580) I*	GAAACTGCACGCTTAAAGCTTG	fgp_139	
		CTTTCCACGTTTCCCGTATC	fgp_140	
		GGGTGATTCGGCAGAAGA	fgp_141	
PPTR-1::GFP	*pptr-1(lt89[pptr-1::gfp])V*	CCTCGGAGAGTACACAAGACC	fgp_158	
		TGGAGTTGTCCCAATTCTTGTT	fgp_2	
		AGCAGCAGAAGACGAGAGAGT	fgp_159	
PPTR-2::GFP	*pptr-2(lt91[pptr-2::gfp])V*	ACGCCCTCAAGATGTTCAT	fgp_160	
		TGGAGTTGTCCCAATTCTTGTT	fgp_2	
		ACTGGGTAAGGAAGTCGAATCA	fgp_161	
AID::GFP::GSP-2	*gsp-2(syb545[AID::gfp::gsp-2])III*	TCTAATTGGGTTGTTTGAGCG	fgp_53	
		TGGAGTTGTCCCAATTCTTGTT	fgp_2	
		TTTTCCCTGGTTTGGATCC	fgp_54	

Supplementary Table 3. List of primers used for genotyping.

	PPTR-1	B56β1	B56β2	B56ε2	B56ε3	B56ε1	B56α2	B56α1	PPTR-2	B56δ1	B56δ2	B56δ3	B56γ4	B56γ5	B56γ1	B56γ2	B56γ3
PPTR-1		60.12	60.08	66.67	71.87	66.59	68.30	63.35	52.26	54.81	56.10	60.17	60.42	57.75	64.48	63.27	59.27
B56β1	60.12		97.56	72.17	73.66	71.83	71.79	69.77	56.36	62.75	63.85	67.13	65.28	64.47	66.21	67.13	64.44
B56β2	60.08	97.56		71.86	73.66	71.52	71.79	69.28	56.59	62.53	63.62	67.13	64.78	63.97	65.68	66.59	63.94
B56ε2	66.67	72.17	71.86		99.74	99.78	78.21	77.49	59.87	66.16	67.60	70.49	67.62	67.81	69.14	69.88	68.75
B56ε3	71.87	73.66	73.66	99.74			79.80	79.80	63.94	71.36	71.36	71.36	73.70	72.38	72.82	73.70	72.38
B56ε1	66.59	71.83	71.52	99.78			78.23	77.52	59.66	65.88	67.28	70.12	67.10	67.27	68.58	69.30	68.19
B56α2	68.30	71.79	71.79	78.21	79.80	78.23		99.07	60.84	67.92	69.14	69.14	71.53	69.56	70.74	71.78	69.79
B56α1	63.35	69.77	69.28	77.49	79.80	77.52	99.07		56.49	63.35	64.97	68.00	66.74	66.37	68.35	69.30	67.49
PPTR-2	52.26	56.36	56.59	59.87	63.94	59.66	60.84	56.49		62.31	61.76	66.19	63.55	60.66	68.97	66.25	62.74
B56δ1	54.81	62.75	62.53	66.16	71.36	65.88	67.92	63.35	62.31		99.65	98.19	79.07	75.68	81.29	80.00	76.72
B56δ2	56.10	63.85	63.62	67.60	71.36	67.28	69.14	64.97	61.76	99.65		98.39	79.72	77.37	82.46	81.05	77.63
B56δ3	60.17	67.13	67.13	70.49	71.36	70.12	69.14	68.00	66.19	98.19	98.39		84.40	81.72	87.62	85.71	81.72
B56γ4	60.42	65.28	64.78	67.62	73.70	67.10	71.53	66.74	63.55	79.07	79.72	84.40		94.57	93.00	93.81	93.61
B56γ5	57.75	64.47	63.97	67.81	72.38	67.27	69.56	66.37	60.66	75.68	77.37	81.72	94.57		92.87	94.64	95.23
B56γ1	64.48	66.21	65.68	69.14	72.82	68.58	70.74	68.35	68.97	81.29	82.46	87.62	93.00	92.87		99.77	98.44
B56γ2	63.27	67.13	66.59	69.88	73.70	69.30	71.78	69.30	66.25	80.00	81.05	85.71	93.81	94.64	99.77		99.79
B56γ3	59.27	64.44	63.94	68.75	72.38	68.19	69.79	67.49	62.74	76.72	77.63	81.72	93.61	95.23	98.44	99.79	

Supplementary Table 1. Percent Identity (%) Matrix of the full length sequence alignment of mammalian B56 isoforms and *C.elegans* orthologues PPTR-1 and PPTR-2 .Created with Clustal Omega version 2.1.

Markers / *mutants*	Strain Number	Genotype	Source
SUR-6::GFP	OD4579	*sur-6(ltl183[GFP::loxP::3xFlag::sur-6]) I*	this study
SUR-6::GFP; mCherry::histone	FGP354	*sur-6(ltl183[GFP::loxP::3xFlag::sur-6])I; ltIs37[pAA64; pie-1p::mCherry::his-58; unc-119 (+)]IV*	this study
GFP::tubulin; mCherry::histone	OD868	*ltSi220[pOD1249/pSW077; Pmex-5::GFP::tbb-2::operon_linker::mCHerry::his-11; cb-unc-119(+)]I*	Wang et al, 2015 (PMID: 24217623)
GFP::tubulin; mCherry::histone; *bub-1(L282A;V285A)*	FGP339	*ltSi220[pOD1249/pSW077; Pmex-5::GFP::tbb-2::operon_linker::mCHerry::his-11; cb-unc-119(+)]I; bub-1(syb1936[bub-1((L282A;V285A)])1*	this study
GFP::tubulin; mCherry::histone; *pptr-2 Δ*	FGP369	*pptr-2(ok1467)V; ltSi220[pOD1249/pSW077; Pmex-5::GFP::tbb-2::operon_linker::mCHerry::his-11; cb-unc-119(+)]I*	this study
GFP::tubulin; mCherry::histone; *bub-1(K718R;D847N)*	FGP337	*ltSi220[pOD1249/pSW077; Pmex-5::GFP::tbb-2::operon_linker::mCHerry::his-11; cb-unc-119(+)]I; bub-1(syb1746[bub-1((K718R;D847N)])*	this study
IFY-1::GFP; mCherry::histone	JAB222	*ify-1(erb-82[ify-1::linker::GFP])II;ltIs37[pAA64; pie-1p::mCherry::his-58; unc-119 (+)]IV; unc-119(ed3)???*	this study
IFY-1::GFP; mCherry::histone; *bub-1(L282A;V285A)*	FGP405	*ify-1(erb-82[ify-1::linker::GFP])II; ltIs37 [pAA64; pie-1p::mCherry::his-58; unc-119 (+)]IV; unc-119(ed3)???; bub-1(syb1936[bub-1(L282A;V285A)])1*	this study
GFP::MDF-1; mCherry::histone	OD2920	*unc-119(ed3)?III; ltIs37[pAA64; pie-1p::mCherry::his-58; unc-119 (+)]IV; mdf-1(lt39[gfp::tev::loxP::3xFlag::mdf-1])V*	Kim et al, 2017 (PMID: 28698300)
GFP::MDF-1; mCherry::histone; *bub-1(K718R;D847N)*	FGP434	*unc-119(ed3)?III; ltIs37[pAA64; pie-1p::mCherry::his-58; unc-119 (+)]IV; mdf-1(lt39[gfp::tev::loxP::3xFlag::mdf-1])V; bub-1(syb1746[bub-1((K718R;D847N)])1*	this study
GFP::MDF-1; mCherry::histone; *bub-1(L282A;V285A)*	FGP426	*unc-119(ed3)?III; ltIs37[pAA64; pie-1p::mCherry::his-58; unc-119 (+)]IV; mdf-1(lt39[gfp::tev::loxP::3xFlag::mdf-1])V; bub-1(syb1936[bub-1(L282A;V285A)])1*	this study
GFP::PAA-1; mCherry::histone	FGP438	*paa-1(syb2267[GFP::linker::paa-1]III; ltIs37[pAA64; pie-1p::mCherry::his-58; unc-119 (+)]IV*	this study
GFP::PAA-1; mCherry::histone; *bub-1(L282A;V285A)*	FGP388	*paa-1(syb2267[GFP::linker::paa-1]III; ltIs37 [pAA64; pie-1p::mCherry::his-58; unc-119 (+)]IV; bub-1(syb1936[bub-1((L282A;V285A)])1*	this study
PPTR-1::GFP	OD3600	*pptr-1(ltl89[pptr-1::gfp])V*	Kim et al, 2017 (PMID: 28698300)
PPTR-1::GFP; mCherry::histone	FGP344	*pptr-1(ltl89[pptr-1::gfp])V; ltIs37 [pAA64; pie-1p::mCherry::his-58; unc-119 (+)]IV*	this study
PPTR-1::GFP; mCherry::histone; *bub-1(K718R;D847N)*	FGP349	*pptr-1(ltl89[pptr-1::gfp])V; ltIs37 [pAA64; pie-1p::mCherry::his-58; unc-119 (+)]IV; bub-1(syb1746[bub-1((K718R;D847N)])1*	this study
PPTR-1::GFP; mCherry::histone; *bub-1(L282A;V285A)*	FGP350	*pptr-1(ltl89[pptr-1::gfp])V; ltIs37 [pAA64; pie-1p::mCherry::his-58; unc-119 (+)]IV; bub-1(syb1936[bub-1((L282A;V285A)])1*	this study
PPTR-1::GFP; mCherry::histone; *san-1Δ*	FGP379	*pptr-1(ltl89[pptr-1::gfp])V;ltIs37 [pAA64; pie-1p::mCherry::his-58; unc-119 (+)]IV; san-1(ok1580) I*	this study
PPTR-2::GFP	OD3424	*pptr-2(ltl91[pptr-2::gfp])V*	Kim et al, 2017 (PMID: 28698300)
pptr-2::GFP; mCherry::histone	FGP317	*pptr-2(ltl91[pptr-2::gfp])V; ltIs37[pAA64; pie-1p::mCherry::his-58; unc-119 (+)]IV*	this study
PPTR-2::GFP; mCherry::histone; *bub-1(K718R;D847N)*	FGP323	*pptr-2(ltl91[pptr-2::gfp])V; ltIs37[pAA64; pie-1p::mCherry::his-58; unc-119 (+)]IV; bub-1(syb1746[bub-1((K718R;D847N)])1*	this study
PPTR-2::GFP; mCherry::histone; *bub-1(L282A;V285A)*	FGP324	*pptr-2(ltl91[pptr-2::gfp])V; ltIs37[pAA64; pie-1p::mCherry::his-58; unc-119 (+)]IV; bub-1(syb1936[bub-1((L282A;V285A)])1*	this study
PPTR-2::GFP; mCherry::histone; *san-1Δ*	FGP380	*pptr-2(ltl91[pptr-2::gfp])V; ltIs37[pAA64; pie-1p::mCherry::his-58; unc-119 (+)]IV; san-1(ok1580) I*	this study

IFY-1::GFP

We utilised CRISPR/Cas9 to generate a C-terminal GFP tagged *C. elegans ify-1* gene, following established protocol (Paix et al., 2015). The repair template, which includes a 5-amino acid flexible linker separating *ify-1*from gfp, was amplified from pDD282, a gift from Bob Goldstein (Addgene plasmid #66823).

GFP::SUR-6

For the generation of in situ-tagged GFP::SUR-6, we used the Self-Excising Cassette method (Dickinson et al., 2015). In brief, N2 adults were injected with a plasmid mix containing Cas9, a sgRNA targeting the N-terminus of sur-6 and a repairing template to insert the GFP sequence, along with a LoxP-flanked cassette that encoded for a hygromycin resistance gene, a sqt-1 mutant to confer a dominant roller phenotype, and heat-shocked-induced Cre recombinase. After selection in hygromycin, positive integrants (evidenced by their roller phenotype) were heat-shocked to express Cre and remove the cassette.

The strains AID::GFP::GSP-2, GFP::PAA-1, BUB-1^{K718R,D847N}, and BUB-1^{L282A,V285A} were generated by Sunybiotech.

AID::GFP::GSP-2

(AID in purple, GFP in green, synonimous mutations in cyan)

ATGCCTAAAGATCCAGCCAAACCTCCGGCCAAGGCACAAGTTGTGGGATGGCCA
CCGGTGAGATCATACCGGAAGAACGTGATGGTTTCCTGCCAAAAATCAAGCGGT
GGCCCGGAGGCGGCGGCGTTCGTGAAGAGTAAAGGAGAAGAACTTTTCACTGGA
GTTGTCCCAATTCTTGTTGAATTAGATGGTGATGTTAATGGGCACAAATTTTCTGT
CAGTGGAGAGGGTGAAGGTGATGCAACATACGGAAAACTTACCCTTAAATTTAT
TTGCACTACTGGAAAACTACCTGTTCCATGGgtaagtttaaacatatatatactaactaaccctgattatttaa

attttcagCCAACACTTGTCACTACTTTCTgTTATGGTGTTCAATGCTTcTCgAGATACC

CAGATCATATGAAACgGCATGACTTTTTCAAGAGTGCCATGCCCGAAGGTTATGT

ACAGGAAAGAACTATATTTTTCAAAGATGACGGGAACTACAAGACACgtaagtttaaac

agttcggtactaactaaccatacatatttaaattttcagGTGCTGAAGTCAAGTTTGAAGGTGATACCCTT

GTTAATAGAATCGAGTTAAAAGGTATTGATTTTAAAGAAGATGGAAACATTCTTG

GACACAAATTGGAATACAACTATAACTCACACAATGTATACATCATGGCAGACA

AACAAAAGAATGGAATCAAAGTTgtaagtttaaacatgattttactaactaactaatctgatttaaattttcagAA

CTTCAAAATTAGACACAACATTGAAGATGGAAGCGTTCAACTAGCAGACCATTA

TCAACAAAATACTCCAATTGGCGATGGCCCTGTCCTTTTACCAGACAACCATTAC

CTGTCCACACAATCTGCCCTTTCGAAAGATCCCAACGAAAAGAGAGACCACATG

GTCCTTCTTGAGTTTGTAACAGCTGCTGGGATTACACATGGCATGGATGAACTAT

ACAAAGACGTAGAAAAGCTTAATCTCGACAATATCATCTCCAGATTATTGGAAG.

GFP::PAA-1

(GFP in green, synonimous mutations in cyan)

ATGAGTAAAGGAGAAGAACTTTTCACTGGAGTTGTCCCAATTCTTGTTGAATTAG

ATGGTGATGTTAATGGGCACAAATTTTCTGTCAGTGGAGAGGGTGAAGGTGATG

CAACATACGGAAAACTTACCCTTAAATTTATTTGCACTACTGGAAAACTACCTGT

TCCATGGgtaagtttaaacatatatatactaactaaccctgattatttaaattttcagCCAACACTTGTCACTACTTT

CTgTTATGGTGTTCAATGCTTcTCgAGATACCCAGATCATATGAAACgGCATGACT

TTTTCAAGAGTGCCATGCCCGAAGGTTATGTACAGGAAAGAACTATATTTTTCAA

AGATGACGGGAACTACAAGACACgtaagtttaaacagttcggtactaactaaccatacatatttaaattttcagGT

GCTGAAGTCAAGTTTGAAGGTGATACCCTTGTTAATAGAATCGAGTTAAAAGGT

ATTGATTTTAAAGAAGATGGAAACATTCTTGGACACAAATTGGAATACAACTAT

AACTCACACAATGTATACATCATGGCAGACAAACAAAAGAATGGAATCAAAGTT

gtaagtttaaacatgattttactaactaactaatctgatttaaatttcagAACTTCAAAATTAGACACAACATTGA

AGATGGAAGCGTTCAACTAGCAGACCATTATCAACAAAATACTCCAATTGGCGA

TGGCCCTGTCCTTTTACCAGACAACCATTACCTGTCCACACAATCTGCCCTTTCGA

AAGATCCCAACGAAAAGAGAGACCACATGGTCCTTCTTGAGTTTGTAACAGCTG

CTGGGATTACACATGGCATGGATGAACTATACAAAGGAGGTGGATCCGGTGGTG

GATCCTCGGTTGTCGAAGAAGCTACTGACGACGCG.

bub-1^{K718R,D847N}

The wild type sequence:

GTAACCGATGATCAAAGGACAGTAGCTGTGAAGTACGAGGTGCCATCATGTTCG

TGGGAAGTGTACATTTGCGACCAAATGCGGAATCGCCTGAAAGATCGAGGTTTG

GAGCTGATGGCCAAATGTTGCATTATGGAAGTGATGGATGCTTATGTTTATTCAA

CTGCTTCGCTTCTTGTTAATCAGTACCACGAATATGGAACGCTGCTTGAATATGC

GAATAACATGAAGGATCCGAATTGGCACATAACCTGCTTCTTGATTACCCAAATG

GCCCGAGTTGTGAAGGAAGTCCATGCCTCTAAAATTATTCATGGAGATATCAAAC

CGGATAATTTTATGATCACCAGAAAgtatgggaaaacatttgttaattttagacgttatctttttcagGATCG

ATGATAAATGGGGCAAAGATGCTCTGATGAGTAACGACAGCTTTGTCATCAAGA

TTATCGACTGGGGACGTGCCATTGACATGATGCCACTGAAGAACCAGCGT

was mutated to:

GTAACCGATGATCAAAGGACAGTAGCTGTGCGCTACGAGGTGCCATCATGTTCG

TGGGAAGTGTACATTTGCGACCAAATGCGGAATCGCCTGAAAGATCGAGGTTTG

GAGCTGATGGCCAAATGTTGCATTATGGAAGTGATGGATGCTTATGTTTATTCAA

CTGCTTCGCTTCTTGTTAATCAGTACCACGAATATGGAACGCTGCTTGAATATGC

GAATAACATGAAGGATCCGAATTGGCACATAACCTGCTTCTTGATTACCCAAATG

GCCCGAGTTGTGAAGGAAGTCCATGCCTCTAAAATTATTCATGGAGATATCAAAC

CGGATAATTTTATGATCACCAGAAAGtatgggaaaacatttgttaattttagacgttatctttttttcagGATCG

ATGATAAATGGGGCAAAGATGCTCTGATGAGTAACGACAGCTTTGTCATCAAGA

TTATCAATTGGGGACGTGCGATTGACATGATGCCACTGAAGAACCAGCGT

The introduced changes are shown in red and synonymous mutations are shown in cyan.

bub-1^{L282A,V285A}

The wild type sequence:

AACGCCAATCTAAATCCTAGAAGACGTCATCTTTCACCAGTCAGTGAGAAAACG

GTTGATGATGAGGAGGAAAAG

was mutated to:

AACGCCAATCTAAATCCTAGAAGACGTCATGCATCACCAGCTAGCGAGAAAACG

GTTGATGATGAGGAGGAAAAG

The introduced changes are shown in red and synonymous mutations are shown in cyan.

See Supplementary Table 3 for the primer sequences used for genotyping.

References

Paix, A., Folkmann, A., Rasoloson, D., and Seydoux, G. (2015). High Efficiency, Homology-Directed Genome Editing in Caenorhabditis elegans Using CRISPR-Cas9 Ribonucleoprotein Complexes. Genetics 201, 47-54.

Dickinson, D.J., Pani, A.M., Heppert, J.K., Higgins, C.D., and Goldstein, B. (2015). Streamlined Genome Engineering with a Self-Excising Drug Selection Cassette. Genetics 200, 1035-1049.